Hydrothermal Alteration and Self-Sealing in Y–7 and Y–8 Drill Holes in Northern Part of Upper Geyser Basin, Yellowstone National Park, Wyoming

GEOLOGICAL SURVEY PROFESSIONAL PAPER 1054–A

Hydrothermal Alteration and Self-Sealing in Y–7 and Y–8 Drill Holes in Northern Part of Upper Geyser Basin, Yellowstone National Park, Wyoming

By TERRY E. C. KEITH, DONALD E. WHITE, *and* MELVIN H. BEESON

HYDROTHERMAL STUDIES IN YELLOWSTONE NATIONAL PARK, WYOMING

GEOLOGICAL SURVEY PROFESSIONAL PAPER 1054–A

UNITED STATES GOVERNMENT PRINTING OFFICE, WASHINGTON : 1978

UNITED STATES DEPARTMENT OF THE INTERIOR

CECIL D. ANDRUS, *Secretary*

GEOLOGICAL SURVEY

V. E. McKelvey, *Director*

Library of Congress Cataloging in Publication Data
Keith, Terry E.
Hydrothermal alteration and self-sealing in Y-7 and Y-8 drill holes in northern part of Upper Geyser Basin, Yellowstone National Park, Wyoming. (Hydrothermal studies in Yellowstone National Park, Wyoming) (Geological Survey Professional Paper 1054-A)
Bibliography: p. 25-26
1. Hydrothermal deposits--Wyoming--Upper Geyser Basin. 2. Borings--Wyoming--Upper Geyser Basin. I. White, Donald Edward, 1914- joint author. II. Beeson, Melvin H., joint author. III. Title: Hydrothermal alteration and self-sealing... IV. Series. V. Series: United States. Geological Survey. Professional Paper 1054-A.
QE475.A2K43 551.3'5 77-608183

For sale by the Superintendent of Documents, U.S. Government Printing Office
Washington, D.C. 20402
Stock Number 024-001-03049-7

CONTENTS

ILLUSTRATIONS

TABLES

HYDROTHERMAL ALTERATION AND SELF-SEALING IN Y–7 AND Y–8 DRILL HOLES IN NORTHERN PART OF UPPER GEYSER BASIN, YELLOWSTONE NATIONAL PARK, WYOMING

By TERRY E. C. KEITH, DONALD E. WHITE, and MELVIN H. BEESON

ABSTRACT

Of the 13 research holes drilled in Yellowstone's thermal areas in 1967 and 1968, 2 holes, Y–7 and Y–8, are the most closely spaced pair, thus providing opportunities for detailed correlations and interpretations of mineralogy and chemistry as affected by differences in original rocks (generally minor), temperatures, pressures, and compositions of the fluid phases. All of these factors, except the detailed fluid chemistry, are considered here.

Y–7 drill hole, with moderately high temperatures and no excess fluid pressures, is outside the present local upflow system. Y–8 drill hole, 130 m away, has temperatures that exceed the simple hydrostatic boiling curve and water overpressures of more than 2.1 kg/cm^2, indicating direct involvement of upflowing fluids. Permeability in obsidian-bearing sands and gravels between the two holes has decreased greatly in response to devitrification, solution, and deposition of hydrothermal minerals, largely in initial pore spaces.

The principal hydrothermal minerals of Y–7 are clinoptilolite, opal, cristobalite, mordenite, and montmorillonitic clays. The more intense alteration of Y–8 includes zones of the same minerals, but in other prominent zones, quartz and analcime have replaced the less stable (more soluble) clinoptilolite and cristobalite; celadonite is the dominant clay mineral. Below −24.8 m in Y–8, hydrothermal potassium feldspar is associated with the analcime-quartz zones, probably having formed from excess potassium as potassium-rich clinoptilolite altered to analcime, quartz, and potassium feldspar.

Local concentrations of calcite in Y–8 are associated with analcime-quartz-potassium feldspar zones in the altered sediments. Rapid upward decrease in fluid overpressure caused boiling, which resulted in partitioning of CO_2 into the vapor phase, and an increase in pH and conversion of bicarbonate to carbonate in the water. Thus, calcite formed by reaction of calcium with carbonate from the water.

The sediments from both drill holes are more altered than the underlying flow breccia of the Biscuit Basin flow, because the initial permeability of the sediments was much greater than that of the flow breccia. The pumiceous tuff of the Biscuit Basin flow is also completely altered to potassium feldspar, quartz, mordenite, and celadonite. The tuff probably had high initial permeability owing to its pumiceous texture, but its permeability is now generally very low.

A detailed study of veinlet mineralogy and paragenesis indicates that first-formed minerals are generally the most soluble and least stable and, in time, are converted into more stable minerals. This succession is most strongly indicated for the five common species of silica minerals.

Major factors influencing formation of the hydrothermal minerals are abundance and reactivity of obsidian as the dominant unstable starting material, temperature, permeability, silica activity, and fluid composition.

The initial lithologies of Y–7 and Y–8 are very similar and indicate high horizontal permeabilities. Thus, present contrasts in wellhead pressures between the two drill holes at equivalent depths provide strong evidence for horizontal self-sealing.

INTRODUCTION

Thirteen diamond-coring research holes were drilled in major thermal areas of Yellowstone National Park in 1967–1968. The physical data obtained from these holes have been described by White, Fournier, Muffler, and Truesdell (1975), but detailed results of petrographic and mineralogic studies have been published only for Y–1 drill hole in Black Sand Basin, in the southwestern part of Upper Geyser Basin (Honda and Muffler, 1970). The local geology has been mapped by Christiansen and Blank (1974), by Waldrop (1975), and by L. J. P. Muffler, D. E. White, and A. H. Truesdell (unpub. data).

This report concerns drill holes Y–7 and Y–8 of Biscuit Basin in the northern part of Upper Geyser Basin, about 2.5 km north of Y–1 (fig. 1) and 3.4 km north-northwest of Old Faithful geyser. Y–7 and Y–8 are the most closely spaced of all the holes drilled by the U.S. Geological Survey, because Y–7 failed to encounter temperatures as high as expected (White and others, 1975, p. 16–17). Y–8 was sited 130 m south of Y–7 near a cluster of hot springs and small geysers, thus ensuring at least localized vigorous upflow and high temperatures. A comparison of the physical data from the two holes (White and others, 1975) provides strong support for the existence of processes that have been called self-sealing, a concept first developed by Bodvarsson (1964) but identified by this term by Facca and Tonani (1967). The present report describes the original rocks and sediments and their conversion by hydrothermal alteration into less permeable rocks by deposition of minerals in fractures and pore spaces.

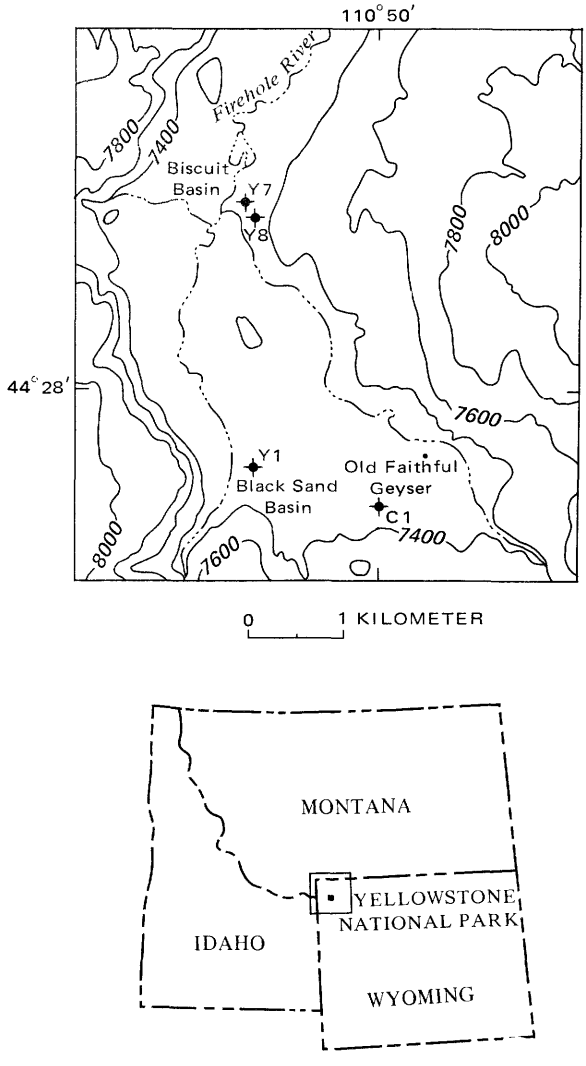

FIGURE 1.—Index map of Upper Geyser Basin, Yellowstone National Park, showing locations of Y–7 and Y–8 research drill holes relative to other holes drilled in the basin. Y–1, Y–7, and Y–8 were drilled by the U.S. Geological Survey in 1967 and C–1 by the Carnegie Institution of Washington in 1929 (Fenner, 1936).

Core recovery from both holes was excellent, except from poorly cemented sediments in the upper parts of Y–7 and Y–8 and an apparently poorly cemented zone from −45.7 to −52.4 m at the base of the sedimentary unit in Y–7. Approximately 20 percent of the total core was selected for laboratory study, with emphasis on obtaining one or more representative samples from each cored interval, generally about 1.5 m, as well as any unusual samples that included veinlets, vugs, or textural extremes. All of the data reported in this paper were obtained from this "skeleton" core. All drill core samples were marked and cataloged by the depth, in feet, at which they were taken in the drill hole; therefore, the sample numbers used in this report refer to downhole depth in feet.

Detailed mineralogical study of the core was made by T. E. C. Keith, utilizing 20 thin sections and more than 70 X-ray diffractograms for Y–7 and 34 thin sections and more than 100 X-ray diffractograms for Y–8. Chemical analyses of minerals were made by M. H. Beeson with an ARL EMX–SM electron microprobe, using natural and synthetic silicate mineral standards. All data were collected on X-ray dispersive spectrometers and corrected for background, matrix absorption, characteristic fluorescence, and atomic number using a modified version of the FRAME IV data reduction program developed at the U.S. National Bureau of Standards (Yakowitz and others, 1973). An excitation potential of 15 kV, a beam current of 0.01 μa (on brass), and a beam diameter of 5 to 10 μm were used in an attempt to produce acceptably high counting rates without destroying the sample. The defocused beam tends to even out inhomogeneities in the samples, but still the average homogeneity index for most elements is relatively large, indicating an inhomogeneous distribution of elements. Chere Bargar provided valuable laboratory assistance in the X-ray studies.

STRATIGRAPHY

The sequence of rocks penetrated by Y–7 and Y–8 drill holes is the same as that of Y–1 (Honda and Muffler, 1970; White and others, 1975) and the Carnegie hole drilled west of Old Faithful in 1929 (Fenner, 1936). The thickness of each stratigraphic unit is similar but not identical in the four holes (table 1).

In this section, we emphasize the original characteristics of the rocks and sediments prior to changes induced by circulating hot water.

SINTER

The shallowest unit is white, gray, and tan sinter, initially consisting of layers of amorphous opaline silica deposited on the ground surface from hot-spring water (as in present-day springs and discharge channels near the drill holes). A few layers, especially from Y–8, are primary sinter consisting of continuous thin beds of amorphous silica that have undergone no conspicuous change since deposition. However, the most abundant type, as in most sinter areas (White and others, 1964, p. B32–B33), consists of angular fragments of primary sinter cemented by amorphous silica. The sinter of both drill holes also contain abundant silicified plant stems, roots, and casts as well as diatoms that are generally rare but locally abundant.

TABLE 1.—*Stratigraphic units penetrated by drill holes in Biscuit Basin compared with other research holes in Upper Geyser Basin*

	Y–7 Biscuit Basin	Y–8 Biscuit Basin	Y–1[1] Black Sand Basin	Carnegie I,[2] Myriad Group
Altitude, surface	2215.2 m (7,266 ft)	2217 m (7,272 ft)	2223.7 m (7,294 ft)	2242.7 m (7,356 ft)
Sinter, thickness	1.8 m (6 ft)	~1.5 m (~5 ft)	3.7 m (12 ft)	~2.2 m (~7 ft)
Altitude at base	2213.4 m (7,260 ft)	2215.5 m (7,267 ft)	2220 m (7,282 ft)	2240.5 m (7,349 ft)
Sediments, thickness	50.9 m (167 ft)	53.7 m (176 ft)	61.0 m (200 ft)	64.9 m (213 ft)
Altitude at base	2162.5 m (7,093 ft)	2161.9 m (7,091 ft)	2159.0 m (7,082 ft)	2175.6 m (7,136 ft)
Biscuit Basin flow				
Flow breccia, thickness	>21.0 m (>69 ft)	7.6 m (25 ft)	>1.2 m (>4 ft)	~13.4 m (~44 ft)
Pumiceous tuff, thickness	Not found	>90.6 m (>297 ft)	Not found	>43.3 m (>142 ft)
Total depth of hole	73.8 m (242 ft)	153.4 m (503 ft)	65.5 m (215 ft)	123.8 m (406 ft)

[1]Honda and Muffler (1970)

[2]Fenner (1936) with additional data from White, Fournier, Muffler, and Truesdell (1975)

A buff-colored silica mud that contains fragments of sinter and fine-grained clastic sediments extends from −1.1 to −1.7 m in Y–7. The variety of sinter known as geyserite is completely absent, thus indicating an absence of geysers and perpetual spouters in the immediate area.

OBSIDIAN-RICH SEDIMENTS

Much of Upper Geyser Basin is underlain by deposits of silt, sand, and gravel. Particle sizes used in this paper are in accordance with the Wentworth scale (Dunbar and Rodgers, 1951, p. 161), except in a few places where our so-called silt actually includes some fine sand. Detrital black obsidian fragments, some with phenocrysts of quartz, sanidine, and plagioclase, comprise the bulk of the sediments. Rounded to subangular rhyolitic fragments, usually pink, purple, or green and consisting of phenocrysts in a groundmass of α-cristobalite[1] and sanidine, are moderately abundant. Detrital mineral grains, originally phenocrysts, are dominantly quartz and sanidine, with subordinate plagioclase and scarce clinopyroxene, magnetite, and zircon. Except for slight cementation, the upper few meters of sediments in both drill holes are similar to the unaltered "black sands" of Upper Geyser Basin except that in Y–7, silicified plant roots are abundant. Deeper in both drill holes, hydrothermal activity has completely reconstituted the obsidian and cemented the detrital fragments into greenish-gray porous sandstone, siltstone, and conglomerate. Coarse- to fine-grained sandstone is the dominant lithologic type; siltstone is relatively abundant as thin interbeds just above the middle, and conglomerate is sporadic in the upper and middle parts and common near the base of the sedimentary units.

Graded bedding and crossbedding are conspicuous in the sands and silts. The bedding is usually subhorizontal or gently dipping, but some crossbeds dip as much as 30° from horizontal (the drill holes are assumed to have been approximately vertical). In Y–7 local small-scale slumping and small faults with as much as 10 mm displacement occur in fine-grained sandstone in core from −21.6 m, and highly contorted beds occur at −23.5 m. Similar small offsets on fractures occur in core from Y–8 at −19.7 m and from −24.8 to −25.0 m.

The sediments were probably outwash stream deposits from and adjacent to receding glaciers of late Pinedale age (Waldrop, 1975; their probable age is from 10,000 to 15,000 years B.P. according to Pierce and others, 1976). The original sediments were mainly silt, sand, and gravel that were sufficiently well sorted to have high porosities and relatively high permeabilities. Even now, the average porosity of sedimentary rocks from the two drill holes, as calculated from bulk and powder densities (table 2), is about 30 percent.

The most likely sources for the obsidian-rich detritus were the Summit Lake flow, which is part of the Central Plateau Member of the Plateau Rhyolite, and the Biscuit Basin and Scaup Lake flows, both of which are part of the Upper Basin Member of the Plateau Rhyolite (Christiansen and Blank, 1972). The obsidian-rich detritus was probably derived largely from the glassy rhyolitic Summit Lake flow, which covers a large area west and southwest of Upper Geyser Basin and has an eruption age of about 127,000 years B.P. (this and other K/Ar ages from J. D. Obradovich, written commun., 1975). Support for this conclusion, as opposed to

[1]In this report the term α-cristobalite is used for the ordered form of cristobalite with major X-ray peak at 4.04 Å and with many other distinct subsidiary peaks. The term β-cristobalite refers to the disordered form with a major broad X-ray peak, generally from 4.06 to 4.12 Å, a second broad peak near 2.50 Å, and commonly with no other distinct peaks. According to Murata and Larson (1975), a complete gradation exists between α- and β-cristobalite, and we find evidence of this in the hydrothermal cristobalites of both Y–7 and Y–8, where the major peak position varies between 4.11 and 4.04 Å.

TABLE 2.—*Chemical analyses of cores from Y–7 and Y–8 drill holes with their unaltered equivalents*

	Scaup Lake flow[1]	Summit Lake flow[1]	Sediments of Upper Basin and dominant source rocks							Biscuit Basin flow			
	Rhyolite	Rhyolite	Y–7 Altered sediments (average of 7)[3]	Y–7–21 Black obsidian gravel and SiO_2[3]	Y–7–142 Volcanic cobble[3]	Y–8 Altered sediments (average of 9)[2,3]	Y–8–14.7 Least altered gravel and SiO_2[3]	Y–8–32.5 Analcime-quartz sandstone[3]	Y–8–160.5 Calcite-analcime-quartz-K-feldspar sandstone[3]	Fresh flow breccia[1]	Y–7 Altered flow breccia (average of 5)[2,3]	Y–8 Altered flow breccia (average of 3)[2,3]	Y–8 Altered pumiceous tuff (average of 4)[2,3]
Major oxides (percent)													
SiO_2	72.95	76.51	71.5	78.9	74.6	70.8	78.6	64.7	72.2	69.86	66.3	64.9	64.2
Al_2O_3	12.50	12.05	11.5	9.8	12.2	12.1	8.6	16.7	11.1	13.11	13.0	13.1	14.3
Fe_2O_3	1.53	.47	.74	.50	1.0	.80	.53	.91	1.1	1.17	1.6	1.9	2.5
FeO	.22	1.11	.44	.64	.36	.41	.52	.36	.44	2.14	1.6	1.2	1.4
MgO	19	.01	.03	.00	.00	.05	.00	.07	.07	.30	.30	.24	.44
CaO	.84	.42	.56	.35	.26	.55	.32	.26	2.5	1.51	1.4	2.0	1.8
Na_2O	3.20	3.65	3.5	2.8	3.8	5.3	2.9	8.6	3.9	3.27	3.5	5.3	4.5
K_2O	5.10	5.10	3.9	4.0	5.3	3.3	3.3	2.9	5.2	4.69	4.2	1.9	4.2
H_2O+	2.37	.23	5.3	2.7	.58	5.1	2.8	5.4	1.5	2.67	5.3	7.1	4.8
H_2O-	.10	.02	2.7	.01	.20	1.7	1.0	.30	.13	.13	2.1	2.6	2.0
TiO_2	.26	.13	16	.12	.12	.15	.10	.16	.19	.45	.46	.47	.53
P_2O_5	.12	01	.05	.04	.05	.07	.06	.07	.06	.09	.14	.15	.16
MnO	.04	.04	.03	.03	.02	.03	.02	.04	.04	.07	.07	.05	.06
CO_2	.01	.01	.03	.03	.03	.04	.02	.02	1.6	.00	.03	.02	.03
Total S as S	.01		.02	.03	.03	.01	.01	.01	.00	.00	.01	.00	.02
Total	99 44	99 76	100	100	99	100	99	100	100	99.46	100	101	101
Bulk density			1.58	2.06	2.31	1.61	2.11	1.51	1.60		1.95	1.99	1.41
Powder density			2.21	2.25	2.44	2.34	2.38	2.35	2.54		2.34	2.28	2.32
Calculated porosity, percent			29	8	5	31	11	36	37		17	13	39
Semiquantitative spectrographic analyses (weight percent)													
B	<0 005	N	<0.0015	0.0015	N	<0.0015	0.003	N	N	N	N	N	N
Ba	.12	.010	.028	.015	.010	.021	.010	.02	.02	.12	.082	.073	.065
Be	N	.0003	.0003	.0005	.0003	.0017	.0002	.005	.002	N	.0003	.0002	.0004
Ce			.014	.010	.010	.013	.015	.015	.010		.015	.012	.010
Co	N	N	N	N	N	N	N	N	N	<.0007	0001	.0001	.0002
Cr	.0003	N	.0001	N	N	.0001	N	.0002	.00015	.0007	.0006	.0006	.0005
Cu	.0003	.0001	.0002	.00015	.0001	.0003	.00015	.0003	.0001	.0005	.0008	.0006	.0008
Ga	.0026	.0018	.002	.003	.002	.0018	.0015	.002	.0015	.0026	.002	.002	.0025
La	010	.013	.010	.007	007	.008	.005	.010	.010	<.005	.008	.009	.007
Li			N	N	N	~.015	N	N	.02		N	N	N
Mo	N	.0007	<.0003	.0003	.0003	N	N	N	N	N	.0002	N	N
Nb	.006	.0079	.003	.002	.005	.003	.002	.003	.003	.003	.002	.002	.003
Pb	.004	.0032	.003	.003	.003	.003	.0015	.003	.005	.003	.002	.003	.003
Sr	.005	.0004	.003	.001	N	.003	.0010	.003	.003	.012	.015	.02	.015
V	.0015	N	N	N	N	N	N	N	N	.002	.0006	.0011	.0010
Y	.0071	.0065	.006	.005	.005	.005	.003	.007	.007	.0057	.007	.007	.008
Yb	0008	.0009	.0005	.0005	.0005	.0005	.0003	.0005	.0007	.0007	.0005	.0005	.0007
Zr	034	.038	.019	.015	.02	.018	.015	.02	.02	.038	.03	.03	.04

[1]Chemical analyses of fresh rocks, from Christiansen and Blank (unpub. data) but excluding F and Cl; analyses of major constituents by standard methods of rock analysis with minor constituents by quantitative spectrographic methods.

[2]Unweighted averages of each major stratigraphic unit; rapid-rock chemical analysis and semiquantitative spectrographic analyses.

[3]Individual analyses by rapid-rock method of Shapiro (1967), Lowell Artis, analyst, and semiquantitative spectrographic analyses, Chris Heropoulos, analyst.

possible derivation from the local Biscuit Basin flow (about 527,000 yrs B.P.) or the Scaup Lake flow (about 265,000 yrs B.P.) which crops out east of Upper Geyser Basin, is found in the petrographic and mineralogic characteristics of the volcanic rocks of the area (R. L. Christiansen, oral commun., 1975). The Summit Lake flow has abundant quartz and sanidine phenocrysts and scarce plagioclase phenocrysts, the Scaup Lake flow has a moderate amount of quartz, sanidine, and plagioclase phenocrysts, and the Biscuit Basin flow has abundant plagioclase and minor quartz and sanidine phenocrysts. The relative abundance of clastic quartz and sanidine grains and paucity of plagioclase grains in the sediments thus support their derivation mainly from the Summit Lake flow. A few of the clastic plagioclase grains in the sedimentary rocks have the same internal sieve texture that characterizes the underlying Biscuit Basin flow, suggesting that this flow supplied a minor amount of the clastic debris.

Additional evidence on the source of the obsidian-rich sediments is provided by chemical and spectrographic analyses of fresh volcanic rocks and hydrothermally altered sediments from the drill holes, summarized in tables 2 and 3. The individual analyses of core from each drill hole are relatively uniform in many constituents in both the sediments and the Biscuit Basin flow. The altered rocks are most nearly similar to the Summit Lake flow in many constituents when corrected for differences in H_2O, suggesting that this rhyolite flow and other chemically similar young flows (Christiansen, unpub. data) supplied most of the sediments. The relatively immobile constituents such

TABLE 3.—*Chemical analyses of altered sedimentary rocks from Y–7, Y–8, and unaltered rhyolite of the Summit Lake flow, recalculated to anhydrous compositions (from table 2)*

	Rhyolite of Summit Lake flow	Y–7 altered sediments with clinoptilolite (average of 7)	Y–8 altered sediments with clinoptilolite (average of 3)	Y–8 altered sediments with analcime (average of 3)
SiO_2	76.89	77.4	75.8	73.0
Al_2O_3	12.11	12.5	12.7	14.6
Fe_2O_3	.47	.8	1.0	.9
FeO	1.12	.5	.4	.4
MgO	.01	.03	.07	.06
CaO	.42	.6	.6	.4
Na_2O	3.67	3.8	5.6	7.1
K_2O	5.13	4.2	3.5	3.4
TiO_2	.13	.17	.19	.17
MnO	.04	.03	.03	.04
Total	99.99	100.0	99.9	100.0
Bulk density		1.58	1.42	1.63
Powder density		2.21	2.24	2.45
Calculated porosity, percent		29	37	34

as TiO_2, P_2O_5, Ba, Cr, and V are especially useful, suggesting that the Scaup Lake flow or the older Biscuit Basin flow may have supplied a small part of the clastic debris. The only immobile constituent that is not easily explained by derivation from the analyzed lava flows is zirconium, which is deficient in the sediments by nearly 50 percent. R. L. Christiansen (oral commun., 1975) has suggested that most zirconium in the rhyolites occurs as zircon phenocrysts; these phenocrysts may have been freed and enriched in near-source sediments.

BISCUIT BASIN FLOW

FLOW BRECCIA

The contact between sedimentary rocks and the underlying flow breccia is abrupt in both holes. This flow breccia and associated pumiceous tuff (in Y–8) are correlated with the Biscuit Basin flow (Christiansen and Blank, 1974), which crops out immediately west of Biscuit Basin and elsewhere in and around Upper Geyser Basin. The pumiceous tuff has not been found in outcrop.

The flow breccia extends from −52.7 m to the bottom of the hole at −73.8 m in Y–7 (table 1), and from −55.2 m to −62.8 m in Y–8. The flow breccia now consists of subrounded fragments of green to black vitrophyre with abundant concentric hydration cracks. The subrounded fragments are enclosed in a similar but lighter green, more altered groundmass. Much obsidian persists in the flow breccia of Y–7, but the flow breccia of Y–8 is more thoroughly altered. The initial flow breccia evidently consisted of angular obsidian blocks (on the order of 5 cm diameter) with interstitial granulated obsidian; the rounded obsidian fragments resulted from hydration that progressed inward from the borders of the angular blocks.

The local flow breccia is pervasively fractured and granulated, and its initial permeability was evidently high enough to permit access of enough water to hydrate the obsidian (table 2) but not high enough for much continued circulation. Initial porosity is not known, but it may have been close to the present porosity of about 14 percent, as calculated from the bulk and powder densities of the drill core.

The obsidian from Y–7 is amorphous to X-rays but has a refractive index ranging from about 1.48 to about 1.50 consistent with the extensive hydration indicated by the chemical analyses. A small amount of α-cristobalite is evident in some X-ray diffraction traces, probably as a product of partial devitrification during initial cooling and prior to the hydrothermal regime. Scarce spherical patches of incipient crystallization of obsidian to α-cristobalite are seen in thin sections of unaltered flow breccia, and an X-ray diffractogram of the same rock shows a small amount of α-cristobalite, comparable to that in the black obsidian of Y–7.

The vitrophyre from the drill holes has a glomeroporphyritic texture with clusters of plagioclase, clinopyroxene, and magnetite; abundant plagioclase and scarce quartz and sanidine occur as solitary phenocrysts. The composition of the plagioclase phenocrysts is about An_{32-35}, as determined by the method of Smith and Yoder (1956). An electron microprobe analysis of a phenocryst in core from Y–8 indicates a composition of $An_{26}Ab_{66}Or_8$. Most of the solitary plagioclase phenocrysts are corroded and have an internal sieve texture (fig. 2). This texture with fresh obsidian

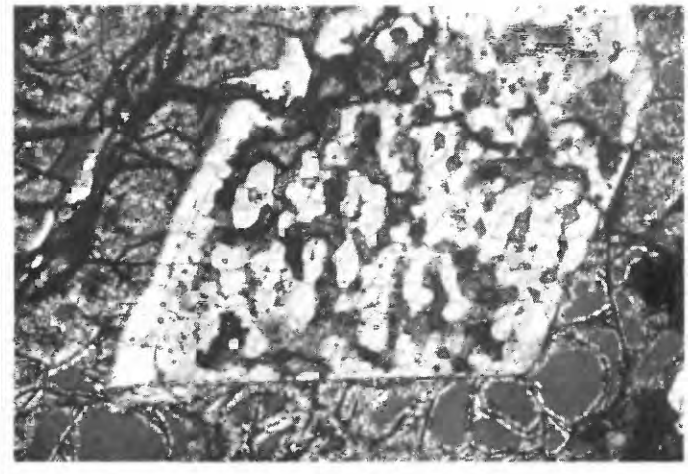

FIGURE 2.—Photomicrograph of perlitic vitrophyre of the Biscuit Basin flow, showing internal sieve texture characteristic of plagioclase phenocrysts. Y–7–238.3 (−72.7 m); partly crossed polars.

filling the holes is characteristic of plagioclase-rich rhyolites of the Plateau Rhyolite, one of which is the Biscuit Basin flow, one of several rhyolite flows within the Upper Basin Member (Christiansen, unpub. data). This texture has clearly resulted from reactions prior to eruption of the lava flow and is unrelated to hydrothermal alteration.

Clinopyroxene phenocrysts of the flow breccia are associated with small euhedral to subhedral magnetite grains and zircon crystals. These mafic clots of crystals occur in unaltered rhyolite of the Biscuit Basin flow and are also primary.

PUMICEOUS TUFF

The pumiceous tuff of the Biscuit Basin flow extends from −63.0 m to the bottom of the hole at −153.4 m in Y–8. The contact with the overlying flow breccia is fairly sharp, occurring within 0.3 m. The pumiceous tuff is light and porous, consisting entirely of pumice fragments generally less than 5 cm in diameter. The porosity of the tuff as calculated from bulk and powder densities is now about 39 percent, which may not differ greatly from initial porosities. The tuff is pale green mottled with dark green; its original color is not known because it does not crop out. Glomeroporphyritic clots of plagioclase, clinopyroxene (now largely replaced by hydrothermal minerals), and solitary plagioclase phenocrysts with the sieve texture shown in figure 2 and an electron microprobe analysis of $An_{26}Ab_{65}Or_9$ provide strong evidence for a close relation between the flow breccia and the pumiceous tuff. The chemical data of table 2 also provide supporting evidence. Most constituents of low mobility, such as titanium, phosphorous, chromium, and zirconium, have nearly identical abundances in the altered pumiceous tuff and in the fresh and altered flow breccia.

The pumiceous tuff has very uniform characteristics at depth in Y–8, with only two exceptions. A thin zone near −113.1 m is fine grained with contorted and slumped bedding, and a crystal-rich layer near −119.5 m (perhaps as thick as 1 m) contains angular to rounded crystals of quartz, plagioclase, scarce sanidine and zircon, and a few lithic rhyolite fragments, but pumice fragments are absent. More thoroughly altered rocks occur in the lower part of Carnegie I drill hole (table 1) and are considered equivalent to the pumiceous tuff of Y–8.

HYDROTHERMAL ALTERATION

The drill core samples from Y–7 and Y–8 are extensively affected by the hydrothermal activity. The duration of the hydrothermal activity in this area is an unsolved problem at present but is likely to have continued for the past 12,000 years or more. The mineralogical changes that are evident, not only in the bulk rocks of Y–7 (fig. 3) but also in associated veinlets, are considerably simpler than in Y–8 (fig. 4) and other previously described core samples from Upper Geyser Basin (Fenner, 1936; Honda and Muffler, 1970). The summary of temperatures, pressures, and implied flow-channels given in figure 5 shows why the rocks of Y–7 should be less affected than Y–8 and thus is described first.

In both drill holes a major focus of interest is the response of rhyolitic obsidian of the "black sand" and the vitrophyric lavas to the thermal environment. Obsidian is a metastable undercooled liquid; in different environments it may remain as obsidian that hydrates in time, it may devitrify to more stable phases, or it may dissolve and allow more stable phases to precipitate in available pore spaces and open fractures. All of these alternatives occur in the Biscuit Basin core.

In this report, the mineralogy of veinlets is discussed separately from that of each hydrothermally altered rock unit. During the earliest hydrothermal activity, the initial sediments were highly permeable. At least partial cementation was first required before crosscutting fractures could form. Thus, the mineralogy of the veinlets may represent somewhat later stages of hydrothermal development than that of the bulk sedimentary rocks.

Y-7 DRILL HOLE

SINTER

Little change has occurred in the sinter since it was first formed. Some of the opal linings of open spaces were deposited from subsurface thermal waters after initial burial.

OBSIDIAN-RICH SEDIMENTS

Obsidian granules, generally hydrated to perlite with concentric hydration cracks, are abundant in sand-sized detritus in the upper part of the hole, and in a conglomeratic zone near −6 m. In general, clastic fragments increase in size downward from −40 m to −48 m with diameters generally ranging from approximately 1 mm to 25 mm. Obsidian remains in the centers of hydrothermally altered clasts in a conglomerate zone at −48.0 m, and as unaltered, probably hydrated, granules in coarse sandstone at −52.7 m. The larger initial volume of glass in individual fragments was probably influential in preserving their centers from attack other than hydration. Elsewhere, most grains are cut by curved fractures that are lined by a variety of minerals, with little or no remaining obsidian.

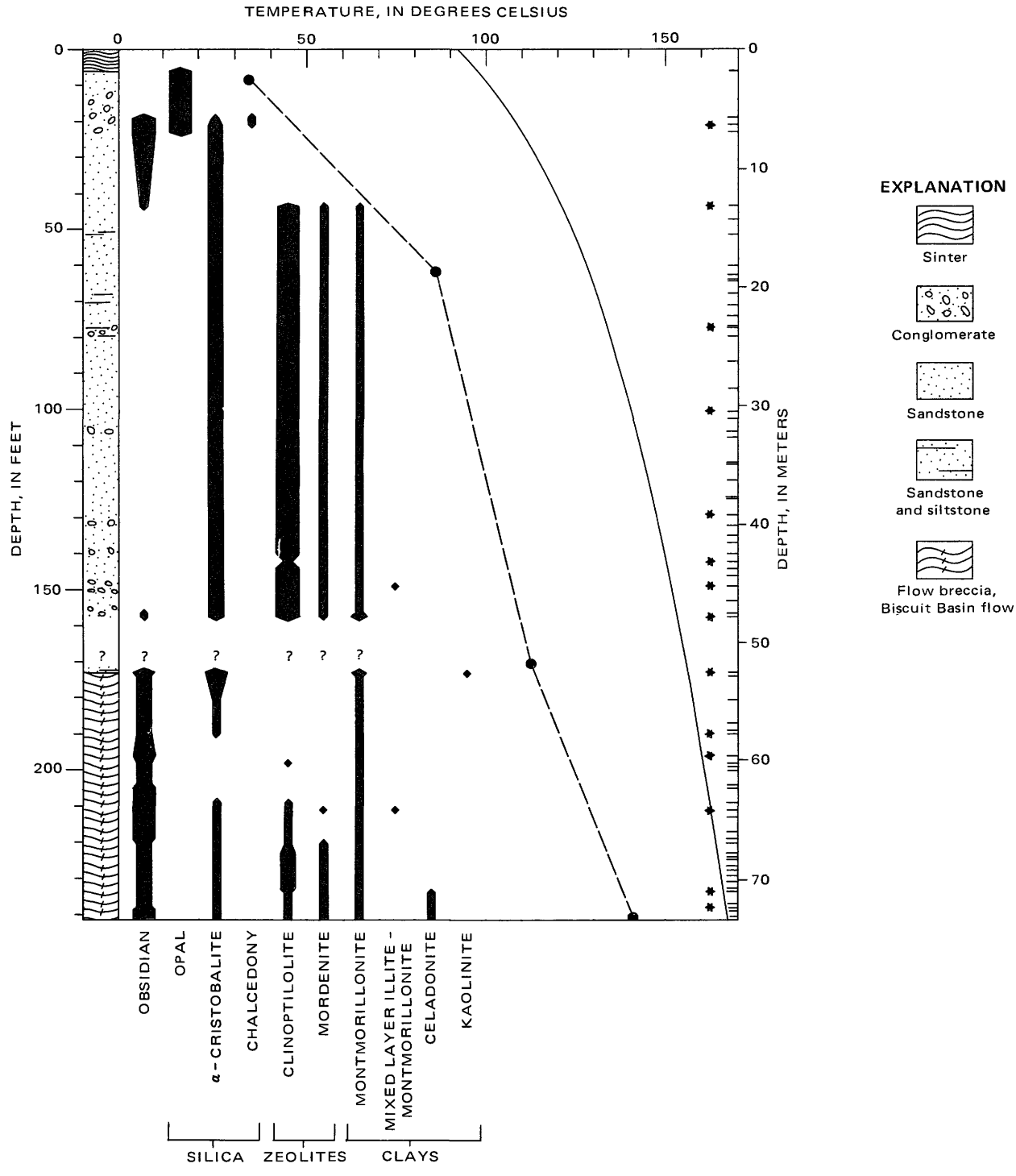

FIGURE 3.—Distribution of fresh obsidian and hydrothermal minerals in groundmass of core from Y–7. Column on left shows generalized stratigraphic section. Horizontal lines at right indicate samples studied in detail, and the starred samples are chemically analyzed. Width of mineral columns shows relative abundance based mainly on X-ray diffraction data and petrographic study. Interpolation between data points assumes linear variation. The dashed line connects data points of bottom-hole temperatures, and the solid line is the reference boiling curve for pure water.

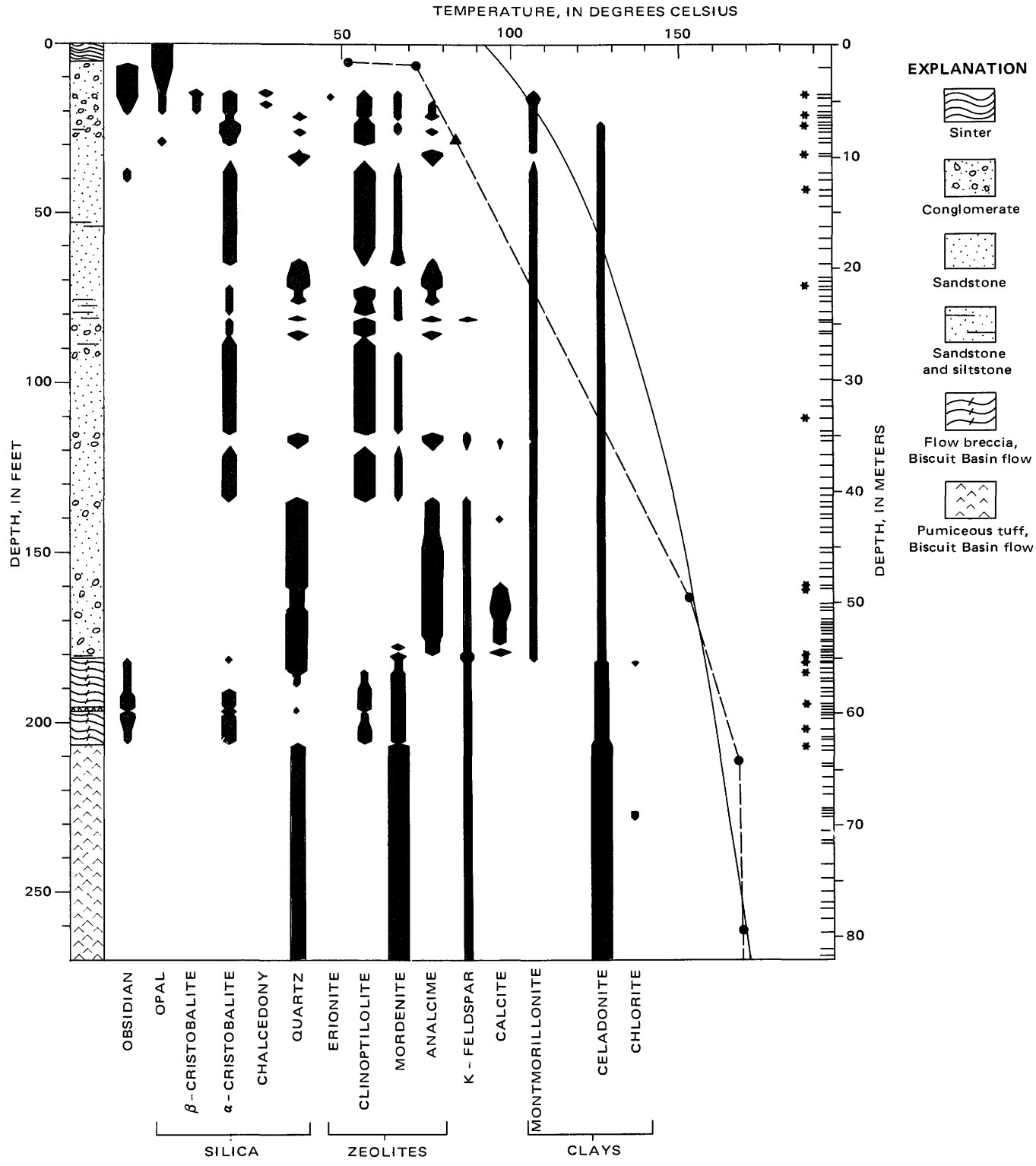

FIGURE 4.—Distribution of fresh obsidian and hydrothermal minerals in groundmass of core from Y–8; data shown in same manner as for Y–7, figure 3. Depths below −82.3 m not shown because of general uniform alteration mineralogy from −63.0 to −153.4 m.

Spherical cavities of similar size and cavities coated with tiny crystals and traversed by curving septa of birefringent minerals are also common. These textures and relict textures characteristic of perlite provide evidence for abundant obsidian granules that were first hydrated to perlite. Hydrothermal minerals then filled the hydration cracks and replaced adjacent hydrated obsidian. Still later, any remaining obsidian either was hydrothermally devitrified or was dissolved, leaving the curving septa as relicts of former hydration cracks and also providing evidence for the sequence of events.

Clear botryoidal amorphous opal occurs as intergranular cement and as thin coatings on most clastic grains in the uppermost conglomeratic zone; many of the grains are obsidian, presumably hydrated. The refractive index of the opal ranges from 1.45 to 1.46. Very small spheres of a mineral of low birefringence are included with opal in figure 3; these spheres may be cristobalite that is too scarce to be identified on X-ray diffraction traces. No amorphous opal was found in the sediments at depths below about −7.5 m. However, veinlet fillings and linings of white to green, nearly isotropic material with the X-ray characteristics of β-cristobalite are especially common from −24.3 to −32.8 m. Because amorphous opal in sinter (White and others, 1964) and diatomite (Murata and Larson, 1975) is converted to β-cristobalite after burial at increased temperatures, we suspect that all β-cristobalite of Y–7 was initially amorphous opal.

The only other silica mineral normally in these sediments is α-cristobalite, which occurs in lithic fragments throughout the unit as a high-temperature devitrification product of the source rhyolite, and also as a hydrothermal mineral. Hydrothermal α-cristobalite is present from −6 to −7 m as small clear spheres of radiating bladelike crystals deposited on an irregular veinlet surface. Chalcedony is a scarce hydrothermal silica mineral, occurring as small white cryptocrystalline patches in intergranular spaces from −5.8 to −6.4 m and as thin coatings of small cavities in a volcanic cobble at −43.3 m (discussed below, and not shown on fig. 3).

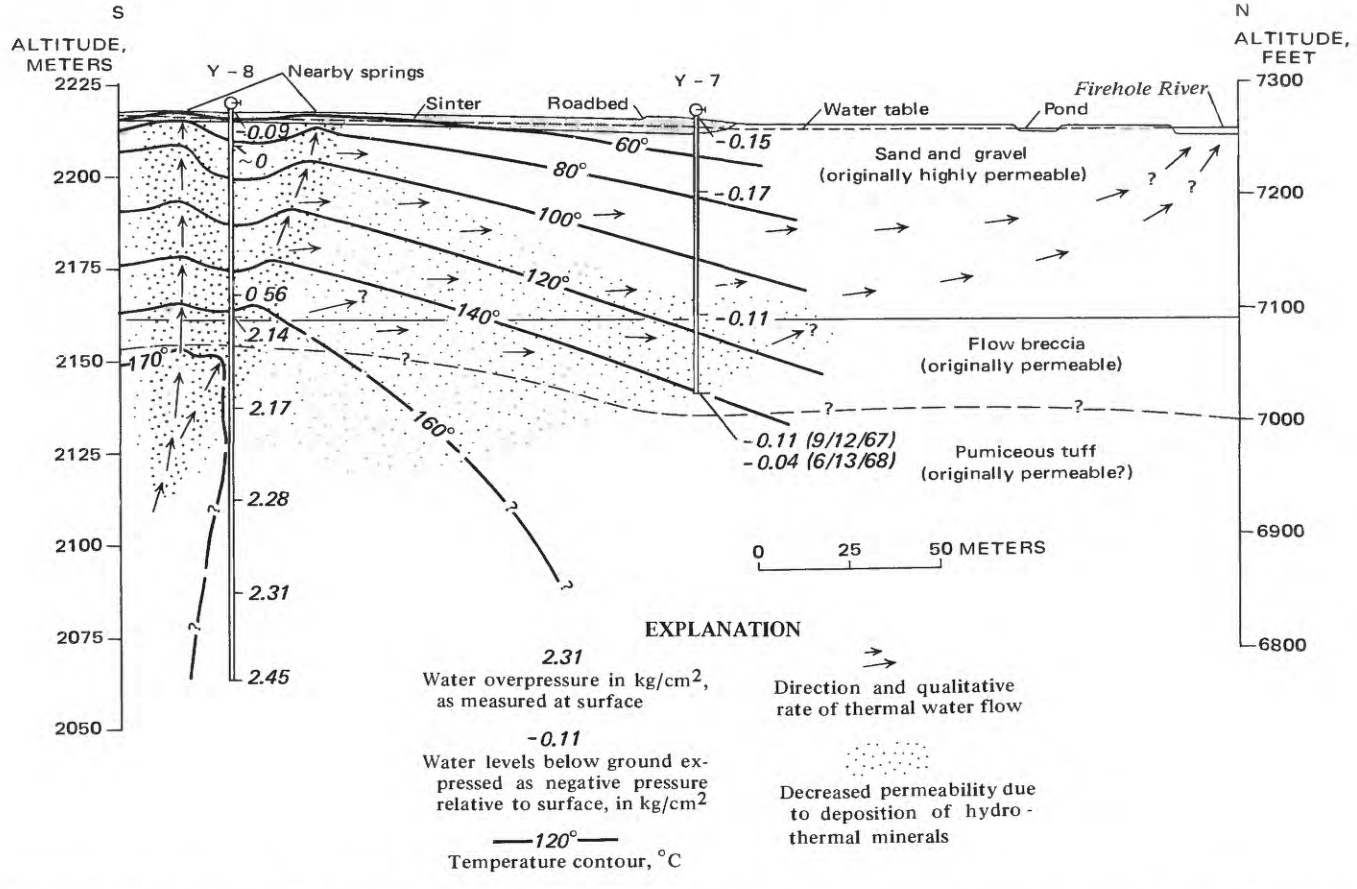

FIGURE 5.—Section through Y–7 and Y–8 drill holes, showing pressures (in kg/cm²), temperature contours, and inferred "self-sealing" by deposition of hydrothermal minerals in originally permeable ground (from White and others, 1975, p. 21).

Hydrothermal alteration and cementation of the sedimentary rocks from −13 to −48 m are relatively uniform (fig. 3). Obsidian either is leached or, more commonly, is replaced by clinoptilolite and montmorillonite. Unfortunately, no core was recovered from the intervals at the top and bottom of this section to provide evidence on mineralogical transitions.

Clinoptilolite is not only a common replacement of obsidian but is also the dominant pore filling mineral that has formed cemented rocks from the clastic sediments. This zeolite also surrounds clastic grains as thin rims of tabular crystals, generally oriented perpendicular to the grain surfaces (fig. 6). Mordenite occurs as hairlike radiating fibers in some pore spaces; it is a subordinate mineral that increases somewhat in amount with depth (fig. 3) and is distinguished optically and by X-ray from the earlier clinoptilolite.

Green montmorillonite occurs throughout the sedimentary section, commonly outlining hydration fractures in altered obsidian and mantled by later clinoptilolite. Concentrations of green to brown montmorillonite also occur in some lithic fragments and altered mafic grains. The X-ray and glycolation characteristics of the clay minerals of Y–7 are summarized in table 4.

Veinlets, dominantly of clay minerals (table 5), are more prominent in the sedimentary rocks of Y–7 than in those of Y–1 (Honda and Muffler, 1970). A little olive-green montmorillonite of normal characteristics (table 4) was deposited in a veinlet at −6.4 m on earlier α-cristobalite. In veinlets at greater depth, the earliest and most prominent mineral is probably montmorillonite, but its X-ray and glycolation characteristics are anomalous for montmorillonite. In untreated samples, this olive-green (or rarely brown) mineral has a 10 Å basal spacing, characteristic of mica and mixed-layer

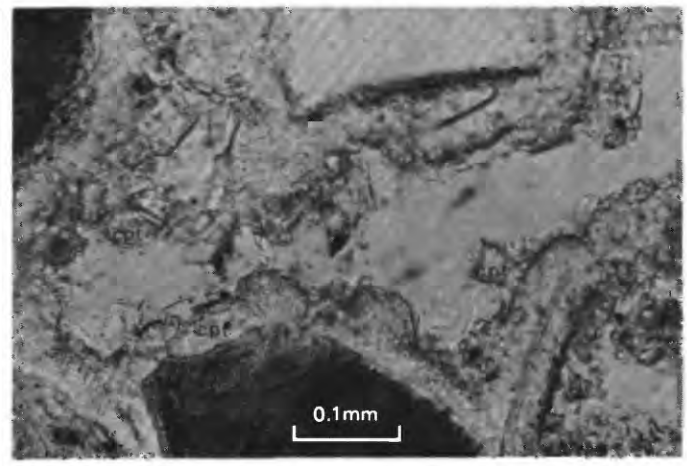

FIGURE 6.—Photomicrograph showing rims of clinoptilolite (cpt) surrounding clastic grains, generally as tiny tabular crystals with long dimension oriented perpendicular to the grain surfaces. Y–7–156.4 (−47.7 m); plane polarized light.

TABLE 4.—*X-ray and glycolation characteristics of clay minerals from Y–7 drill hole, with identifications used in this report*

Sample No.[1]	Description	Untreated	Glycolated ½ hour at 60°C	Heated ½ hour at 400°C	Identification
Sedimentary unit					
Y7–21.0–4	Olive-green clay in veinlet	12.6 Å (broad)	17.6 Å	----	Montmorillonite
Y7–47.2–1	do.	10.0 Å	17.6 Å	----	10 Å expanding clay
Y7–64.0–1	do.	10.05 Å	17 Å	9.9 Å	Do.
Y7–64.0–2	do.	10.0 Å	19.6 Å	----	Do.
Y7–73.8–1	do.	10.2 Å	19.2 Å	----	Do.
Y7–94–2	Brown clay in veinlet	10.0 Å	19.6 Å (broad)	9.8 Å	Do.
Y7–94–3	Olive-green clay in veinlet	10.05 Å	17 Å	9.9 Å	Do.
Y7–94–4	Red Fe-stained clay in veinlet	10.07 Å (broad)	17 Å	10.2 Å	Do.
Y7–115–1	Olive-green clay in veinlet	10.6 Å	16.9 Å	9.8 Å	Do.
Y7–119.5–1	do.	10.05 Å	17 Å	9.8 Å	Do.
Y7–124–1	do.	10.5 Å	17.3 Å	----	Do.
Y7–149–1	Altered perlite fragment	11.0 Å	10 Å and broad at higher d-spacing	----	Interlayered montmorillonite-celadonite
Y7–157.5–1	Green clay in veinlet	10.9 Å	16.9 Å	9.8 Å	10 Å expanding clay
Y7–173	Silt, groundmass	16.99 Å	16.99 Å	9.8 Å	Montmorillonite
Y7–173	do.	7.13 Å	----	7.13 Å	Kaolinite
Flow breccia, Biscuit Basin flow					
Y7–174–3	Altered groundmass	13.3 Å (broad)	17.3 Å	----	Montmorillonite
Y7–180.5–1	Thin coating gray-green clay	12.2–14.4 Å (broad)	17.3 Å	10 Å	Do.
Y7–190	Groundmass	12.2 Å (broad)	17.3 Å	9.8 Å	Do.
Y7–198–1	Orange-yellow altered glass	11.6 Å	11.3 Å (broad)	11.3 Å (broad)	Montmorillonite (?)
Y7–205–1	Yellow waxy coating	11.9 Å (weak)	17.6 Å (broad, weak)	10 Å (small)	Montmorillonite
Y7–209–1	Green clay in veinlet	No distinct maximum	Shifts to higher d-spacing and 10.0 Å	9.8 Å	Interlayered montmorillonite-celadonite
Y7–209–2	Groundmass	11.6 Å	18.4 Å (broad)	11.0 Å (broad)	Montmorillonite
Y7–211	do.	11.0 Å (broad)	17.3 Å, 9.8 Å (weak)	9.9 Å	Interlayered montmorillonite-celadonite
Y7–217–1	Veinlet coating	11.9 Å	12.2 Å and broad at higher d-spacing	12.1 Å	Do.
Y7–229.2–1	Groundmass	12.9 Å (broad)	17.6 Å	----	Montmorillonite
Y7–233.6–1	do.	12.9 Å	18.4 Å (broad)	----	Do.
Y7–237–4	Dark-green clay from veinlet	10.6 Å	9.8 Å	----	Celadonite
Y7–241.6–1	Dark-green veinlet	10.28 Å	10.04 Å	10 Å	Do.

[1]Sample number corresponds to depth in feet.

illitic clays (table 4). However, upon glycolation, the mineral expands to or near the 17 Å spacing expected of montmorillonite, with little or no indication of a 10 Å mica component. Because of uncertain identity, this mineral is called "10 Å expanding clay". In core from −6.4 m, −52.7 m, and from the underlying flow breccia, most of the expanding clays show the normal characteristics of montmorillonites with untreated d-spacings from about 12 to 15 Å, similar to those of Y–1 (Honda and Muffler, 1970).

Several veinlets in the middle and lower part of the sedimentary section contain β-cristobalite, either as the only mineral or later than the 10 Å expanding clay. Tiny crystals of pyrite, where present, are the latest hydrothermal mineral. Pyrite has not been identified in the groundmass of the sedimentary rocks. Zeolites are notably absent in veinlets from this drill hole, in contrast to the abundant clinoptilolite and common mordenite of the adjacent sedimentary rocks.

The core from −43.3 m, consisting entirely of dense dark-green fine-grained rhyolite, is interpreted to be a lithic volcanic cobble rather than a thin flow within the sediments. It is described here rather than in the foregoing systematic discussion of the sedimentary rocks because its mineralogy and chemical composition (table 2) indicate high-temperature devitrification and vapor-phase reactions associated with extrusion in a rhyolite flow, with only minor hydrothermal effects after its incorporation as a cobble in the sediments. A few phenocrysts of sanidine and quartz occur in a devitrified groundmass of α-cristobalite and sanidine that probably formed during initial cooling. Euhedral tridymite and sanidine occur in small irregular cavities and are interpreted as high-temperature vapor-phase precipitates in vesicles. Overlying these minerals in some small cavities are thin layers that were deposited in the sequence of celadonite, clinoptilolite, mordenite, and chalcedony, all of which were probably deposited in the active geothermal system. The key minerals supporting this interpretation are the euhedral tridymite and sanidine in cavities; the high bulk density and low water content (table 2) also point to high-temperature devitrification, and the chemical aspects of the cobble are similar to rhyolite of the Summit Lake flow.

A critical gap in recovered core extends from −48.0 to −52.7 m. A single piece of core from −52.7 m contains an upper layer of coarse- to medium-grained sandstone consisting dominantly of black obsidian clasts. The underlying layer is light-buff siltstone that

TABLE 5.—*Distribution and sequence of deposition of hydrothermal minerals in veinlets of Y–7 drill hole*

[Numerical order indicates sequence of deposition in each veinlet. Query indicates uncertain order of deposition. --, not found]

Sample[1] No.	Interlayered montmorillonite celadonite	Montmorillonite	10 Å expanding clay	Celadonite	Chalcedony	α-cristobalite	β-cristobalite	Opal	Clinoptilolite	Calcite	Mordenite	Acicular unknown	Pyrite
Sedimentary unit													
Y7–21.0	--	2	--	--	--	1	--	--	--	--	--	--	--
Y7–47.2	--	--	1	--	--	--	--	--	--	--	--	--	--
Y7–64.0	--	--	1	--	--	--	--	--	--	--	--	--	--
Y7–64.4	--	--	1	--	--	--	--	--	--	--	--	--	--
Y7–73.8	--	--	1	--	--	--	--	--	--	--	--	--	2
Y7–79.6	--	--	--	--	--	--	1	--	--	--	--	--	--
Y7–94.0	--	--	1	--	--	--	2	--	--	--	--	--	3
Y7–107.5	--	--	--	--	--	--	1	--	--	--	--	--	--
Y7–115.0	--	--	1	--	--	--	--	--	--	--	--	--	--
Y7–119.5	--	--	1	--	--	--	--	--	--	--	--	--	--
Y7–124.0	--	--	1	--	--	--	--	--	--	--	--	--	--
Y7–124.5	--	--	1	--	--	--	--	--	--	--	--	--	--
Y7–157.5	--	--	1	--	--	--	2	--	--	--	--	--	3
Flow breccia, Biscuit Basin flow													
Y7–198.0	--	--	--	--	--	--	1	--	2	--	--	--	--
Y7–199	--	--	--	--	--	--	1	--	--	--	--	--	--
Y7–200	--	--	--	--	--	--	1	--	--	--	--	--	--
Y7–209	1	--	--	--	3?	2?	4	5	6	7	8	--	--
Y7–211	1	--	--	2	--	3	4	--	5	--	6	--	--
Y7–213	--	--	--	--	--	--	1	--	2	3	--	--	--
Y7–217	1	2	--	--	--	--	3	4	5	--	--	--	--
Y7–219	1	--	--	--	--	--	2	3	4	--	--	--	--
Y7–219a	1	--	--	--	--	--	2	3	--	--	--	--	--
Y7–219b	1	--	--	--	--	--	--	--	2	--	--	--	--
Y7–220.3	1	--	--	--	--	--	--	--	2	--	3	4	--
Y7–223	1	--	--	--	--	--	--	--	2	--	3	4	--
Y7–224.8	1	--	--	--	--	--	--	--	2	--	3	4	--
Y7–227.7	1	--	--	--	--	--	2	--	3	--	4	--	--
Y7–229.2	1	2	--	--	--	--	3	--	4	--	5	--	--
Y7–233.6	--	--	--	1	--	--	2	--	3	--	4	--	--
Y7–237	--	--	--	1	--	--	2	3	4	--	5?	6?	--
Y7–238.3	--	--	--	1	--	--	2	3,5	4	--	6	--	--
Y7–239	--	--	--	1	2	3	6	7	4	--	--	5	--
Y7–239a	--	--	--	1	--	2	--	--	3	--	4	--	--
Y7–239.3	--	--	--	1	--	--	2	3	--	--	4	--	--
Y7–240.6	--	--	--	1	--	--	2	3	4	--	5	--	--
Y7–241	--	--	--	1	--	--	2	3	4	--	5?	6?	--

[1]Sample number corresponds to depth in feet

now consists mainly of montmorillonite (fig. 3 and table 4) with subordinate α- and β-cristobalite, quartz, sanidine, and kaolinite. No zeolites or mixed-layer clays were detected. A chemical analysis (not included in table 2) shows major and minor constituents that are intermediate in content between the overlying sediments and the underlying Biscuit Basin flow, suggesting local derivation of some of the clastic debris. Kaolinite was identified from this depth (table 4 and fig. 3) but not elsewhere in this drill hole.

FLOW BRECCIA OF THE BISCUIT BASIN FLOW

The vitrophyric flow breccia of Y–7 is extensively altered in its upper part, least altered from −62 to −67 m, and increasingly altered downward to the bottom of the hole at −73.7 m. Much of the groundmass consists of thoroughly hydrated obsidian, which is amorphous to X-rays and has an average total water content of about 7 percent (table 2). The altered groundmass from −53.0 to −59.8 m contains light-green montmorillonite that has totally replaced obsidian. Light-blue or gray-green montmorillonite fills hydration cracks in the remaining obsidian. The montmorillonites of various colors are poorly crystalline and have similar X-ray characteristics (table 4). The groundmass from −60.4 to −62.5 m is altered to an orange-yellow material that is nearly amorphous to X-rays, is optically isotropic, and is possibly equivalent to the light-green, poorly crystalline groundmass montmorillonite at deeper levels.

From −63.7 m to the bottom of the hole at −73.7 m, clinoptilolite is the dominant groundmass mineral along with subordinate green montmorillonite. Below −67 m, mordenite becomes conspicuous, and celadonite appears to increase below −71.2 m. In order of deposition, the paragenetic sequence consists of (1) green montmorillonite (and celadonite below −71.2 m) replacing obsidian along hydration cracks; and (2) clinoptilolite progressively replacing part of the remaining obsidian and crystallizing in the hydration cracks as subhedral crystals on the montmorillonite and oriented perpendicular to the cracks. Residual obsidian was locally leached, with clinoptilolite and (or) mordenite then being deposited in the leached cavities. The initial stages of alteration of obsidian are illustrated by figure 7, and the progressive filling of an adjacent pore space, part of a veinlet serving as a permeable channel, is illustrated by figure 8.

Obsidian that initially filled the holes of sieved plagioclase phenocrysts (see fig. 2) is now replaced by α-cristobalite and finely crystalline green interlayered celadonite-montmorillonite in the upper part of the unit, and by celadonite in the lower part. Fibers of mordenite may fill the remaining parts of the nonfeldspar framework. The plagioclase shows no alteration or change in composition and is evidently more stable than the obsidian. Clinopyroxene phenocrysts are not stable, generally being partly replaced by green clay minerals. Irregular and subhedral grains of magnetite and euhedral crystals of zircon are primary phenocrysts, although the magnetite may have minor hydrothermally deposited overgrowths of an unidentified opaque oxide.

The mineralogy and sequence of deposition in the veinlets of the flow breccia are summarized in table 5.

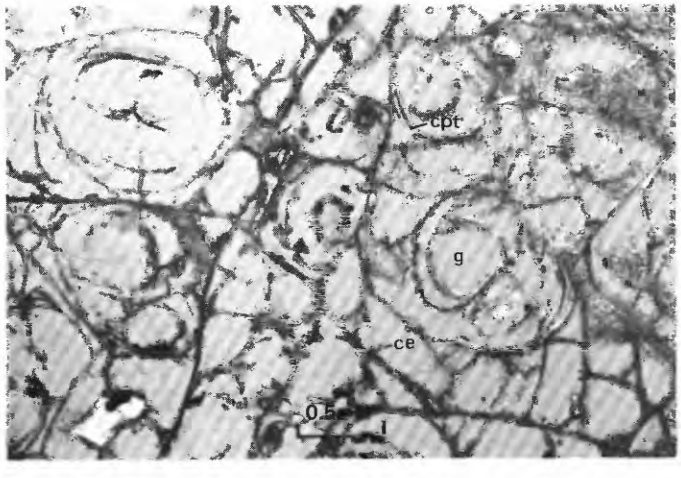

FIGURE 7.—Photomicrograph showing initial stages of alteration of obsidian (g) to celadonite (ce, dark) and clinoptilolite (cpt, birefringent) adjacent to perlitic cracks. Y–7–238.3 (−72.6 m); partly crossed polars.

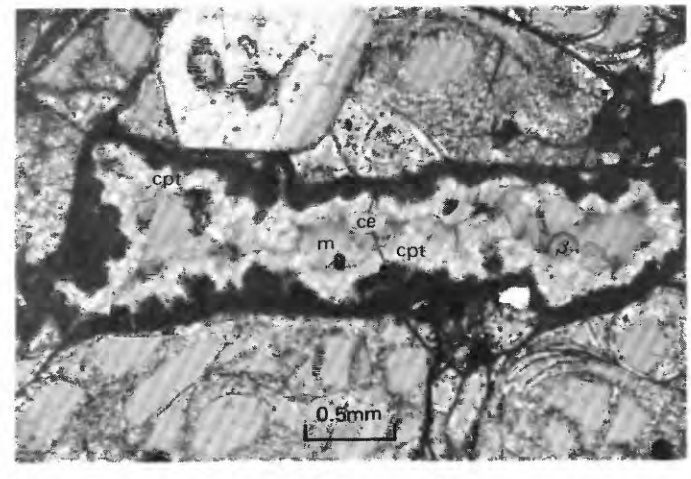

FIGURE 8.—Photomicrograph of the area adjacent to figure 7, showing progressive increase in alteration toward veinlet filled with celadonite (ce), clinoptilolite (cpt), β-cristobalite (β), and mordenite (m). Y–7–238.3 (−72.6 m); partly crossed polars.

The veinlets range in width from less than 0.5 mm to about 8 mm; the wider veinlets are not everywhere completely filled with hydrothermal minerals. The mineral assemblages in these veinlets are generally more complex than those in the groundmass of the flow breccia and in the veinlets of the overlying sedimentary unit. The veinlet mineralogy of the flow breccia does not everywhere correlate with the groundmass mineralogy (for example, a thin coating of clinoptilolite forms a veinlet at −60.4 m, but the adjacent groundmass contains no zeolites). Silica minerals, along with green clay minerals, are the most abundant constituents of the veinlets, but clinoptilolite (also with green clay minerals) is the dominant replacement of the obsidian groundmass.

The earliest mineral of the veinlets is generally green mixed-layer celadonite-montmorillonite near the top of the flow breccia (tables 4 and 5) and, below −70 m, celadonite with little or no mixed layering. Pale-green and blue-white varieties of β-cristobalite are generally the next minerals in sequence, commonly followed by a thin layer of clear isotropic opal that seems still to be amorphous. Locally, chalcedony and α-cristobalite precede the β-cristobalite. Clinoptilolite is almost universally present, generally occurring as small tabular crystals on earlier β-cristobalite. Radiating fibers of mordenite are later than clinoptilolite and, in the middle and lower parts of the unit, are locally followed by tiny clear radiating acicular crystals of an unidentified mineral. In its five known occurrences in the drill hole, the unidentified mineral is closely associated with mordenite, and, from its optical properties and X-ray powder camera data, is probably also a zeolite.

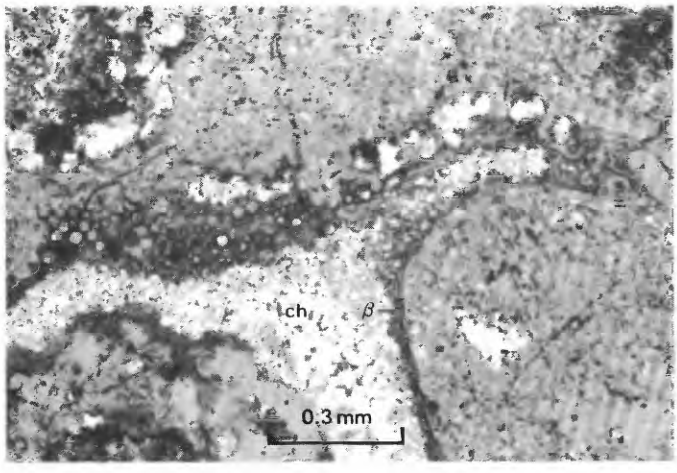

FIGURE 9.—Photomicrograph showing pore spaces between clasts in conglomerate filled by spheres of early-formed opal (o), thin bands of nearly isotropic β-cristobalite (β), and later chalcedony (ch) from nearby veinlet. Y–8–18.0 (−5.5 m); partly crossed polars.

Calcite occurs locally as a late veinlet mineral at −63.7 and −64.9 m. Pyrite, as in the bulk rock, is absent.

Y–8 DRILL HOLE

SINTER

The uppermost 0.2 m consists of layers of coherent mottled white and gray fragmental sinter with a few thin bands of primary sinter. Deeper core to −0.6 m consists entirely of gray fragmental sinter. As at Y–7, geysers and perpetual spouters were probably absent in the immediate area.

No core was recovered from −0.6 to −4.3 m, but a sample of loose grains that include both obsidian sand and sinter was obtained from −2.1 m, so that contact is presumably at a slightly shallower depth, arbitrarily placed at −1.5 m. The fragments of sinter are cemented with clear opal, thus indicating some effects of circulating thermal waters after burial.

OBSIDIAN-RICH SEDIMENTS

As in Y–7, obsidian is preserved mainly in the upper part of the sedimentary section, preferentially in the larger clasts. A little obsidian persists in sand-size grains near −12.2 m but was not detected in any of the deeper sedimentary layers (fig. 4). Elsewhere in Y–8, relict concentric hydration cracks indicate a former abundance of obsidian that hydrated to perlite.

α-cristobalite is probably present in part as a high-temperature devitrification product within the obsidian grains, but its qualitative abundance in the zones in which it occurs (fig. 4) suggests that it is also in part a hydrothermal mineral. Amorphous opal occurs locally in the upper 9 m of Y–8 (fig. 9). β-cristobalite was identified in the groundmass only in the upper 6 m of Y–8 and is absent at greater depths, in striking contrast to its distribution in Y–7. Chalcedony and quartz are abundant in some zones of Y–8.

Of the four zeolite minerals identified in the sedimentary section, erionite is the rarest, occurring only in a single sample from −4.9 m. This rarity is similar to its sparse occurrence only in the upper 15 m of Y–1 (Honda and Muffler, 1970).

Clinoptilolite is the dominant zeolite in most of the middle and upper parts of the sedimentary section, where it replaces obsidian and also occurs in pore spaces as tabular crystals 20 to 70 μm long, generally with long dimensions oriented perpendicular to clastic grain surfaces. Clinoptilolite is strikingly absent below −41 m, where analcime is abundant. Mordenite is a common but generally not an abundant associate of

clinoptilolite; mordenite also accompanies analcime in the upper part of the hole, but these two zeolites are rarely associated at depths below −24 m.

As noted by Honda and Muffler (1970) in Y–1, analcime is typically associated with hydrothermal quartz or chalcedony but rarely accompanies the less stable (more soluble) forms of silica. The association pairs of analcime-quartz (or chalcedony) and clinoptilolite-cristobalite (either variety, but mainly α-cristobalite) are nearly mutually exclusive and alternate irregularly in subhorizontal zones with depth. These zones are roughly parallel to the sedimentary bedding, and boundaries are rather sharp. However, a few analcime grains extend very slightly into clinoptilolite zones, but clinoptilolite crystals have not been observed extending into analcime-quartz zones. The thickness of individual zones ranges from about 2 mm (in the intervals from −5.5 to −7.9 m, and from −22 to −23.2 m) to 12.5 m. The zones show no clear relation to initial particle size or composition in the clastic sediments.

Conspicuous overgrowths of hydrothermal quartz and potassium feldspar occur on clastic mineral grains, beginning at about −24.8 m and continuing downward throughout the sedimentary unit in the analcime-quartz zones. The most common overgrowth is quartz on clastic quartz in optical continuity, but hydrothermal potassium feldspar occurs as overgrowths on clastic sanidine and also on clastic plagioclase (fig. 10). The overgrowths generally differ slightly in optical relief from the clastic grains and also generally include other tiny hydrothermal mineral grains, especially near the original grain boundaries. In some thin sections from quartz-analcime zones, tiny euhedral hydrothermal potassium feldspar crystals about 20 to 40 μm wide and with rhombic cross sections typical of adularia are visible along with the euhedral quartz as cavity linings.

Green clay minerals occur throughout the sedimentary section as replacements of perlitic glass along concentric hydration cracks and also as cryptocrystalline massive clots that apparently replace volcanic lithic fragments and clastic ferromagnesian minerals. In thin section several types of clay are apparent: (1) light-green color and moderately low birefringence, probably a montmorillonite; (2) brown to orange-brown color and moderate birefringence, probably a montmorillonite; and (3) strong deep-green color and moderately high birefringence, probably celadonite. These identifications are supported by X-ray diffraction and glycolation characteristics, summarized in table 6. The clay types coexist as separate minerals and probably also as mixed-layer celadonite-montmorillonite. However, the distribution of montmorillonite and celadonite is shown in figure 4 as separate clays, mainly from thin-section observations.

Calcite, absent in the sedimentary section of Y–7, is abundant in Y–8, especially in the lower part of the thick basal analcime-quartz zone from −50 to −55 m. The calcite typically occurs as white blades with pearly luster, generally as a late filling of pore spaces (fig. 11).

Veinlet minerals in the sedimentary section of Y–8 consist dominantly of chalcedony and, rarely, quartz, sometimes followed by analcime, mordenite, or rhombic calcite (table 7). All of the veinlets are in analcime-quartz zones except at −22.1 m, which is in a clinoptilolite zone but immediately below an analcime-quartz zone. This veinlet is also unusual in

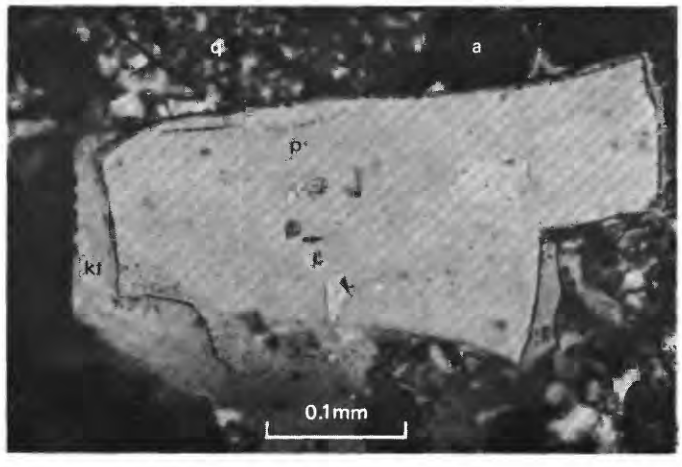

FIGURE 10.—Photomicrograph showing overgrowth of hydrothermal potassium feldspar (kf) on clastic plagioclase grain (p), with intergranular quartz (q) and analcime (a). Y–8–169.5 (−51.7 m); partly crossed polars.

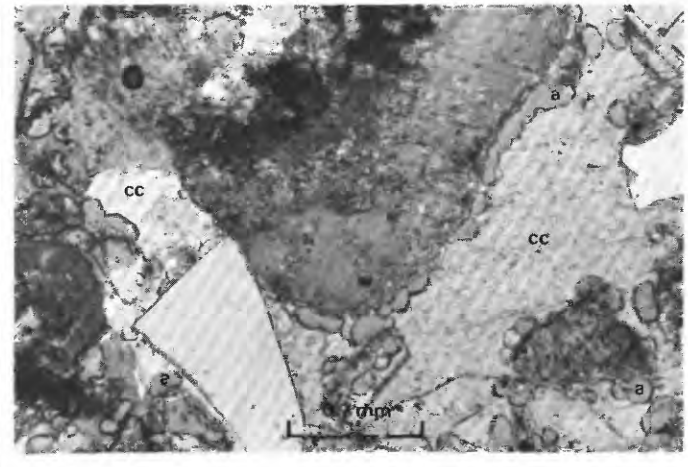

FIGURE 11.—Photomicrograph showing late pore filling of calcite (cc) deposited on analcime (a) in sandstone. Y–8–169.5 (−51.7 m); partly crossed polars.

containing chalcedony with clinoptilolite. Analcime in Y–8 veinlets occurs where the adjacent groundmass contains analcime. The dominant silica mineral of the veinlets is usually chalcedony, whereas quartz is usually dominant in the adjacent groundmass. β-cristobalite was identified in a veinlet only at −7.0 m, in contrast to its distribution to −32.8 m in Y–7. Clay minerals are notably absent in the veinlets of Y–8 in contrast to Y–7, where clays are the dominant veinlet fillings and zeolites are absent.

FLOW BRECCIA OF THE BISCUIT BASIN FLOW

Vitrophyric flow breccia extends from −55.2 m to −63.0 m, except for a thin interbed of pumiceous tuff or granulated pumice at −59.9 m. From −63.0 m to the bottom of the hole at −153.4 m, the rocks consist of relatively homogeneous pumiceous tuff, all of which has been extensively altered hydrothermally.

The flow breccia was initially similar to the same unit previously described from Y–7. Obsidian that is only partially devitrified and hydrothermally altered is characteristic of the middle third of the unit, where as much as 50 percent of the obsidian persists. The upper and lower parts of the flow breccia have generally decreasing proportions of residual obsidian toward the contacts of the unit (fig. 4) as the hydrothermal minerals increase in abundance.

Quartz is prevalent in the groundmass from −55 to −56 m and is generally sparse or absent elsewhere. Below −56.4 m, α-cristobalite and clinoptilolite are the characteristic groundmass minerals of hydrothermal origin, having replaced obsidian. Calcite, abundant in the immediately overlying sedimentary rocks, decreases strikingly downward in the flow breccia and was not identified below −55.8 m. Deep-green celadonite is the characteristic clay mineral of the unit (table 5); chlorite was identified only from −55.6 m, where chlorite and celadonite occur together. Thin layers of bright-green celadonite fill hydration cracks of the altered groundmass. Clinoptilolite, directly replacing the glass, forms a layer of fibrous and sometimes tiny tabular crystals on celadonite oriented perpendicular to the cracks. Later tabular clinoptilolite crystals, and in a few places fine fibrous mordenite, were deposited on earlier clinoptilolite where the obsidian granules are completely replaced or dissolved.

Obsidian that initially filled the holes of the sieved plagioclase phenocrysts has been replaced by α-cristobalite and celadonite (fig. 2). Mordenite is a late-stage deposit in some holes. Pure potassium feldspar occurs as patches forming internal rims or

TABLE 6.—*X-ray and glycolation characteristics of clay minerals from Y–8 drill hole, with identifications used in this report*

Sample[1] No.	Description	Untreated	Glycolated ½ hour at 60°C	Heated ½ hour at 400°C	Identification
Sedimentary unit					
Y8–15.7–1	Light yellow-green clay in porous areas	11.6 Å	17.8 Å	10.0 Å	Montmorillonite
Y8–27.8–1	Very minor clay in groundmass	10.2 Å	10.0 Å, 17.6 Å	----	Celadonite and montmorillonite
Y8–32.2–2	Hard green veinlet	10.0 Å, 11.0 Å, 11.9 Å	9.9 Å, 11.0 Å (broad)	10.0 Å, 11.0 Å	Celadonite and montmorillonite (?)
Y8–64.6–1	Green clays in groundmass	10.2 Å, 12.45 Å	10.2 Å, 16.3 Å	10.2 Å	Celadonite and montmorillonite
Y8–64.6–2	do.	9.9 Å, 11.1–13.5 Å	10.0, 13.3, 16.3 Å	10.0 Å, 11.0 Å	Do.
Y8–69.7–1	do.	9.9 Å, with broad shoulder to greater d-spacing	9.0 Å, 12.6–13.19 Å	10.0 Å	Do.
Y8–81.4	do.	10.0 Å, with broad shoulder to greater d-spacing	10.0 Å, 16.0–17.6 Å (broad)	----	Do.
Y8–82–1	Groundmass clays	10.0 Å	10.0 Å, 17.6 Å	----	Do.
Y8–85.4–1	do.	10.1 Å, 12.6 Å	10.0 Å, 13.8 Å	10.0 Å	Do.
Y8–140–2	do.	10.1 Å, 13.1 Å	10.1 Å, 14.1 Å	----	Do.
Y8–177.6–1	do.	10.1 Å, 13.5 Å	10.2 Å, 16.9 Å	----	Do.
Flow breccia, Biscuit Basin flow					
Y8–182.2–2	Groundmass clays	10.0 Å, 14.0 Å, 7.0 Å	9.9 Å, 14.0 Å, 7.0 Å	----	Celadonite and chlorite
Y8–182.2–3	do.	10.0 Å, 7.0 Å (small)	9.9 Å, 7.1 Å (small)	----	Do.
Y8–185.3–1	Dark-green veinlet	10.2 Å	10.0 Å	9.9 Å	Celadonite
Y8–185.3–2	Green clay in groundmass	10.1 Å	9.9 Å	10.0 Å	Do.
Pumiceous tuff, Biscuit Basin flow					
Y8–304–1	Dark-green veinlet	10.1 Å	10.0 Å	10.0 Å	Celadonite
Y8–327–1	Red center of veinlet	10.2 Å	9.8 Å	10.0 Å	Do.
Y8–327–2	Green borders of same veinlet	10.2 Å	9.9 Å	10.0 Å	Do.
Y8–327–3	Groundmass clay	10.1 Å	10.0 Å	----	Do.
Y8–331.2–1	do.	10.1 Å	10.0 Å	10.0 Å	Do.
Y8–335	do.	10.2 Å	9.9 Å, 11.9–14 Å (broad)	----	Celadonite with minor interlayered montmorillonite
Y8–371–1	Black, fine-grained zone in groundmass	10.2 Å	10.0 Å	9.9 Å	Celadonite
Crystal tuff					
Y8–391.8–1	Buff groundmass clay	12.1–14.1 Å (broad) 7.02 Å	16.6 Å, 14.0 Å, 7.05 Å	10.0 Å, 7.05 Å	Montmorillonite and chlorite
Y8–391.8–2	Green groundmass clay	10.5 Å, 7.08 Å	9.9 Å, 7.08 Å	----	Celadonite and chlorite

[1]Sample number corresponds to depth in feet.

overgrowths in the holes within the sieved plagioclase and also fills microfractures extending outward from the holes. Beam scans with the electron microprobe confirm the composition and distribution of the potassium feldspar and thus its probable hydrothermal origin.

Clinopyroxene phenocrysts are partially to completely replaced by celadonite. Associated magnetite and zircon, as in Y–7, are probably primary phenocrysts. However, an unidentified opaque phase (hematite?) is seen in reflected light filling microfractures in magnetite grains and as irregular partial overgrowths or replacement at grain boundaries. This opaque phase is very scarce but indicates some hydrothermal alteration of the magnetite.

Veinlets of hydrothermally deposited minerals are relatively abundant in the flow breccia, generally ranging from 0.5 to 4 mm in width; the wider veinlets are commonly not completely filled. The most abundant minerals are celadonite, β-cristobalite, opal, and mordenite. The sequences of deposition are generally consistent in trend in the different veinlets, with only a few reversals (table 7). No single veinlet contains the full sequence; a few veinlets are monomineralic (generally celadonite), and three veinlets contain as many as seven of the ten species recognized in the unit.

The flow breccia adjacent to the wider veinlets is generally completely altered, with the hydrothermal effects generally decreasing away from the veinlets, as in Y–7.

The earliest mineral of nearly all veinlets is dark-green botryoidal celadonite (fig. 12). Near the top of the flow breccia, celadonite occurs with fine-grained quartz (table 7), but elsewhere celadonite is either alone or is followed by cristobalite and one or more zeolites, most commonly mordenite.

TABLE 7.—*Distribution and sequence of deposition of hydrothermal minerals in veinlets of Y–8 drill hole*

[Numerical order indicates sequence of deposition in each veinlet. Query indicates uncertain order of deposition.—, not found]

Sample[1] No.	Celadonite	Goethite	Quartz	Chalcedony	α-cristobalite	β-cristobalite	Opal	Clinoptilolite	Analcime	Laumontite	Mordenite	Calcite (rhombic)	Calcite (bladed)	Pyrite
Sedimentary unit														
Y8–18.0	--	--	--	1	--	--	--	--	--	--	--	--	--	--
Y8–21.5	--	--	--	1	--	--	--	--	--	--	--	--	--	--
Y8–23	--	--	--	1	--	2	--	--	--	--	--	--	--	--
Y8–32.2a	--	--	--	--	--	--	--	--	--	--	1	2	--	--
Y8–32.2b	1?	--	--	2?	--	--	--	--	3	--	--	--	--	--
Y8–32.5	--	--	--	1	--	--	--	--	2	--	3	--	--	--
Y8–33	--	--	--	1	--	--	--	--	2	--	3	--	--	--
Y8–69.7	--	--	2	--	--	--	--	--	1	--	--	3	--	--
Y8–70	--	--	--	1	--	--	--	--	--	--	--	2	--	--
Y8–72.5	--	--	--	2	--	--	--	1	3	--	4	--	--	--
Y8–76	--	--	--	1	--	--	--	--	--	--	--	--	--	--
Y8–81.4	--	--	--	1	--	--	--	--	--	--	--	--	1	--
Y8–166	--	--	--	--	--	--	--	--	--	--	--	--	2	--
Y8–170.5	--	--	1	--	--	--	--	--	--	--	--	--	2	--
Y8–171	--	--	1	--	--	--	--	--	--	--	--	--	2	--
Y8–180	--	--	--	1	--	--	--	--	--	--	2	--	--	--
Flow breccia, Biscuit Basin flow														
Y8–181.9	--	--	--	1	--	--	--	--	--	--	2	--	--	--
Y8–185.3	1	--	2,5	3	--	--	--	--	--	--	4	--	--	--
Y8–185.3a	1	--	--	--	--	--	--	--	3	--	2	--	--	--
Y8–187	1	--	2	--	--	--	--	--	--	--	3	--	--	--
Y8–187a	--	--	--	--	--	--	--	--	1	--	2	--	--	--
Y8–188	1	--	2	--	--	3	4	--	--	--	--	--	--	--
Y8–188a	1	--	--	--	--	--	--	--	--	--	--	--	--	--
Y8–190	1	--	--	--	--	3	4	2,5	--	6	7	--	--	--
Y8–191.1	1	--	--	--	--	2	3	--	--	--	4	--	--	--
Y8–191.1a	1	--	--	--	--	--	--	--	--	--	--	--	--	--
Y8–192.3	1	--	--	--	--	2	3	--	--	--	4	--	--	--
Y8–192.3a	1	--	--	--	--	--	--	--	--	--	--	--	--	--
Y8–194.5	1	--	--	--	--	3	4	2	--	--	--	--	--	--
Y8–195.5	1	--	--	--	--	2	--	--	--	--	--	--	--	3
Y8–197.3	--	--	--	--	--	1	2	--	--	--	3	--	--	--
Y8–197.7	1	--	3	--	2	4	--	--	--	6?	5?	--	--	--
Y8–199	1	--	--	--	2	--	3	4	--	5?	6?	--	--	--
Y8–199a	1	--	--	--	--	--	--	--	--	--	--	--	--	--
Y8–202	1	--	--	--	2	--	--	--	--	--	3	--	--	--
Y8–204.3	1	--	--	--	--	--	--	--	--	--	--	--	--	--
Y8–205	1	--	--	--	--	--	--	--	--	--	2	--	--	--
Pumiceous tuff, Biscuit Basin flow														
Y8–226.3	--	--	--	--	--	--	--	--	1	--	2	--	--	--
Y8–236	--	--	--	--	--	--	--	--	1	--	2	--	--	--
Y8–247	--	--	--	--	--	--	--	--	--	--	1	--	--	--
Y8–294	1	--	--	--	--	--	--	--	--	--	2	--	--	--
Y8–304	1	--	--	2	--	--	--	--	--	--	--	--	--	--
Y8–327	1	2?	--	3?	--	--	--	--	--	--	--	--	--	--
Y8–331.2	--	1	--	2	--	--	--	--	--	--	--	--	3	--
Y8–350	1	--	--	--	--	--	--	--	--	--	--	--	--	--
Y8–354	--	--	--	--	--	--	--	--	--	--	1	--	2	--

[1]Sample number corresponds to depth in feet.

The five recognized species of silica minerals are never present in a single veinlet, but three species occur together at −57.3 and −60.3 m; most other veinlets have two species. The sequence of deposition is generally from the most stable phase, quartz, to the least stable (most soluble) phase, opal. β-cristobalite is the most abundant silica phase and forms a bluish-white botryoidal layer (fig. 12).

Mordenite is moderately abundant and is the last mineral to have been deposited in most veinlets; it is not associated with any particular assemblage. Neither clinoptilolite nor analcime is common in veinlets, in contrast to the abundant clinoptilolite that has replaced obsidian of the flow breccia. Laumontite, not previously described from the rhyolitic rocks of Yellowstone National Park but common elsewhere in many calcium-rich geothermal systems, was identified in three veinlets from −58 to −61 m by X-ray diffraction and optical properties. The laumontite occurs as very small prismatic crystals and is mixed with mordenite.

A minor amount of subhedral pyrite occurs in a veinlet at −59.6 m. The groundmass of the crystal tuff at −119.5 m contains the only other pyrite identified in Y–8.

PUMICEOUS TUFF OF THE BISCUIT BASIN FLOW

The contact of flow breccia and underlying pumiceous tuff occurs at about −63.0 m, but the actual contact was not recovered in core. The whole unit of pumiceous tuff is relatively uniform and consists of soft, punky, fine-grained tuff with glomeroporphyritic clusters of plagioclase and clinopyroxene, and with only a few crosscutting veinlets. The tuff is pale green mottled with dark-green patches that are enriched in celadonite and abundant white patches that are largely mordenite.

The hydrothermal alteration of the pumiceous tuff is extensive and relatively uniform. The groundmass consists dominantly of hydrothermal celadonite and mordenite that have replaced initial glass of the pumice (fig. 13). In most of the other Yellowstone drill core, mordenite is a common minor constituent of zeolitic assemblages, but in the pumiceous tuff, it is the only identified zeolite. The frothy pumice texture is preserved although alteration is complete. Anhedral to euhedral hydrothermal quartz crystals, averaging about 30 μm in length, are present throughout the unit. α-cristobalite is present from about −92.7 to −99.7 m as hemispheres deposited between celadonite and some of the later mordenite and is again characteristic below −120 m.

Tabular euhedral to subhedral crystals of potassium feldspar, about 20 to 40 μm long, are associated with mordenite fibers throughout the tuff, and all are presumed to be hydrothermal. Analysis by electron microprobe of the crystals from −92.9 m indicates a composition of $Or_{97}Ab_3An_0$, which provides very strong support for a hydrothermal rather than devitrification or vapor-phase reaction origin.

Tiny clusters of chlorite have crystallized on celadonite that has entirely replaced augite phenocrysts from

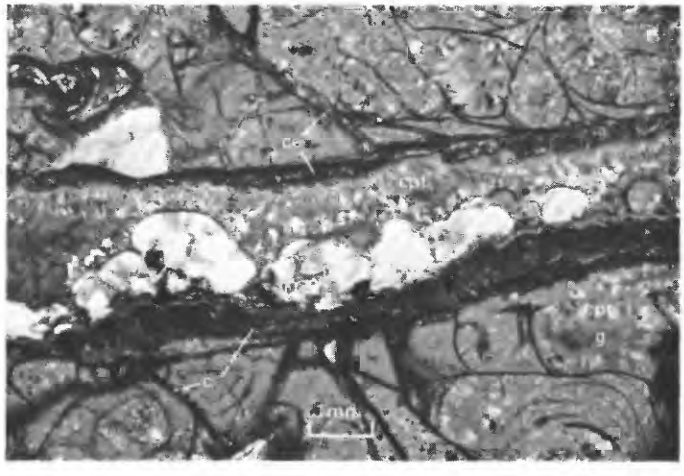

FIGURE 12.—Photomicrograph of veinlet consisting of early dark green celadonite (ce) and later botryoidal β-cristobalite (β) and clinoptilolite (cpt). Perlitic glass (g) of groundmass is almost entirely replaced by celadonite and clinoptilolite. Y–8–190 (−57.9 m); partly crossed polars.

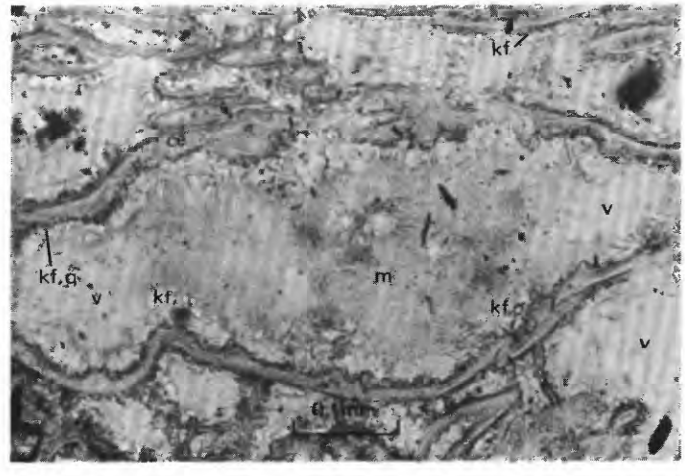

FIGURE 13.—Photomicrograph showing frothy pumice texture preserved and outlined by dark-green celadonite (ce) which has replaced initial glass. Tiny euhedral crystals of quartz (q) and potassium feldspar (kf) have crystallized on celadonite, and mordenite (m) has filled much of the pore space (v). Y–8–304B (−92.7 m); plane polarized light.

−68.9 to −69.5 m. No other chlorite has been identified in the pumiceous tuff. A few dark-green aphanitic volcanic rock fragments enriched in celadonite are scattered throughout the tuff.

Many solitary plagioclase phenocrysts have the same sieve texture as described for the vitrophyric flow breccia of Biscuit Basin, but the obsidian within the feldspar framework has been dissolved and mordenite, celadonite, and hydrothermal potassium feldspar deposited. Clinopyroxene phenocrysts are completely replaced by celadonite, which crudely retains the clinopyroxene crystal outlines. Associated magnetite, as in other parts of this Biscuit Basin flow, is probably primary.

A thin zone near −119.5 m is enriched in subrounded crystals of quartz, sanidine, plagioclase, and minor magnetite and zircon. Most of the crystals are close to 0.75 mm in diameter. Also included are a very few rhyolite fragments, but no obsidian or pumice was recognized. Intergranular hydrothermal minerals are montmorillonite, celadonite, and chlorite (table 5). Scarce intergranular pyrite is dispersed throughout the zone. Internal bedding appears to be nearly horizontal, although neither the upper nor the lower contact was recovered. This local zone is probably a crystal tuff.

From −120 m to the bottom of the drill hole at −153.4 m, the pumiceous tuff is very uniform in appearance. The characteristic hydrothermal minerals are mordenite and celadonite, and minor potassium feldspar, α-cristobalite, and quartz.

Veinlets are not abundant in the pumiceous tuff, but, where present, they affect the adjacent groundmass. As in the overlying flow breccia, celadonite and mordenite are the most abundant veinlet minerals (table 7), but celadonite is not nearly so abundant. The mineral assemblages tend to be less complex than in the open veinlets of the overlying flow breccia. No veinlet contains more than three of the six mineral species recognized in veinlets of the unit. The veinlets range in width from less than 0.5 mm to about 4 mm, and most are completely filled with hydrothermal minerals. Veinlets are completely absent in the basal 34 m of pumiceous tuff below the crystal tuff at −119.5 m.

Celadonite, where present, is the earliest veinlet mineral. Mordenite, the only common zeolite, was deposited on clear euhedral analcime in two veinlets at −68.9 and −72.0 m. Analcime also occurs in thin subparallel veinlets as much as 20 mm below the thickest veinlet at −68.9 m. Goethite, not recognized elsewhere, is a relatively early mineral in two veinlets near −100.6 m (table 7). Later chalcedony is the only recognized silica species. Calcite is known to occur only in one veinlet at −101.0 m, and the adjacent tuff is silicified 6 cm from the veinlet to a hard gray rock mottled with green celadonite. A silicified zone about 8 cm thick at −113.1 m consists of steeply dipping, hard, dark-gray layers of chalcedony.

SIGNIFICANCE OF MINERALS AND MINERAL ASSEMBLAGES

OBSIDIAN

Obsidian was initially abundant in the sediments and in the Biscuit Basin flow. Because glass is metastable (an undercooled liquid) it tends to be highly reactive and provides constituents for minerals that are stable (or less unstable) in the existing environment. The first reaction is hydration of nonperlitic obsidian, initially with less than 0.3 percent water (table 1, Summit Lake flow; Friedman and Smith, 1958). Perlitization occurs when water is absorbed from the environment, and the consequent progressive increase in volume causes outer shells to expand and spall, forming the onion-skin layers. Most perlites in nonthermal environments have water contents ranging from about 2 to 5 percent. The least altered of the obsidian-bearing sediments from Y–7 and Y–8 (table 2) contains 2.7 percent total H_2O, and the least hydrated vitrophyric flow breccia contains 5.8 percent total H_2O; both of these are in large part perlite.

Only a little undevitrified obsidian or perlite remains in the sedimentary section, persisting down to −7.0 m in Y–7 and −4.6 m in Y–8 (figs. 3 and 4). However, minor obsidian occurs sporadically at greater depths in the sediments of both drill holes (figs. 3 and 4).

Obsidian is still abundant in the flow breccia, especially in the central parts of the unit in both drill holes, and thus has persisted at temperatures that are considerably higher than in most of the overlying sediments where the obsidian granules are completely reconstituted. Temperature is obviously not the only factor that controls the conversion of obsidian to more stable minerals.

Hydrothermal alteration of obsidian granules progresses inward from grain boundaries and along and adjacent to hydration cracks. An increase in volume occurs when anhydrous obsidian is hydrated, and further increases occur during reconstitution to zeolites and clay minerals. Clinoptilolite is one of the few hydrothermal minerals that require little chemical change other than addition of water as obsidian is devitrified. Most hydrothermal minerals require a major local chemical change, with some constitutents being added from the pore fluid as the other constituents are removed, either by means of a through-going fluid or by precipitation nearby as new minerals. The grain

density of the rock decreases progressively through hydration and reconstitution wherever hydrothermal alteration changes do not add quartz, calcite, and feldspar in sufficient proportions to affect the decreasing density.

Permeability of the sediments and the borders of the flow breccia must have been initially high, judging from fresh viscous zones, flows, and flow breccia elsewhere. The preservation of abundant undevitrified but hydrated obsidian in the vitrophyric flow breccia at temperatures as high as 170°C is probably a consequence of the decreased porosity and permeability that resulted from initial hydration and incipient alteration along hydration cracks. The absence of wholesale replacement of obsidian by clinoptilolite in the sediments, as well as the preservation of hydrated obsidian in the vitrophyric flow breccia, may also be due to an inadequate supply of additional water; an increase in water content from about 5 to 9 percent is necessary to produce clinoptilolite from hydrated obsidian. Diffusion rates are too slow to supply much of the needed water, except over the short distances adjacent to the rare permeable channels such as veinlets. We have no good explanation for the complete absence of zeolites in the upper 7.6 m of the flow breccia of Y–7 (fig. 3); zeolites do occur in this part of the unit in Y–8 (fig. 4).

CLAY MINERALS

Clay minerals were the first direct replacements or reconstitutions of obsidian in and adjacent to fractures and hydration cracks. Clay patches were also deposited in pore spaces prior to most zeolites.

X-ray data on the groundmass clays were difficult to obtain owing to their very small grain size and poor crystallinity, but data on clays in veinlets are good. Optical data on clays in any sample are quite variable and not diagnostic except for the well-crystallized celadonites in the Biscuit Basin flow. The clays are generally distinguished as montmorillonite or celadonite, as determined by X-ray diffraction (tables 4 and 6). Irregularly mixed layer clays are probably also commonly present, but these can seldom be distinguished.

The poorly defined mineral identified in tables 4 and 5 as "10 Å expanding clay" is the most abundant clay of the sedimentary unit in Y–7 and is included with normal montmorillonite in figure 3. Scanty chemical and electron microprobe data indicate that much potassium has been absorbed without producing a nonexpanding illite structure. We cannot be certain that any of the clays analyzed with the electron microprobe are the "10 Å expanding clay". However, we have two semiquantitative spectrographic analyses on samples studied by X-ray diffraction, and these both show potassium as the dominant large cation. We suspect, but cannot prove, that this mineral is an intermediate step between montmorillonite and celadonite; we do not understand its restriction to this unit in Y–7 or why similar clays have not been recognized elsewhere.

Electron microprobe analysis shows the clays in the sedimentary unit to have a large compositional variation between and within grains (table 8, fig. 14). The average homogeneity index, $\frac{\sigma}{\sqrt{\bar{N}}}$, (Boyd, 1969) indicates large variations within grains. Only CaO has a homogeneity index low enough to be due to statistical variation in the counting system of the electron microprobe. All of the green clays contain appreciable but variable amounts of K_2O, and none of the analyzed green clays contains less than 3.26 percent K_2O. Whether the low-potassium clays represent montmorillonite "stuffed" with K_2O, or whether they are

TABLE 8.—*Electron microprobe analyses of clay minerals from Y–7 and Y–8*
[Analyst: M. H. Beeson]

	Average[1] brown clay from sedimentary unit	Range	Average[2] green clay from sedimentary unit	Range	Average[3] $\frac{\sigma}{\sqrt{\bar{N}}}$ for green clay	Y–8–194.5 Dark-green celadonite in veinlet	Y–8–194.5 Clay "blebs" in replacement clinoptilolite	Y–8–194.5 Celadonite after clinopyroxene
SiO_2	61.3	60.6 –61.9	64.8	53.3 –80.3	14.3	55.9	40.3	59.2
Al_2O_3	9.4	6.0 –10.9	8.7	4.0 –11.6	6.7	10.7	10.2	10.1
MgO	.05	.04– .06	.25	0 – .92	6.3	1.64	1.12	1.90
'FeO'[4]	3.19	1.4 – 5.0	4.02	.8 – .94	8.6	12.3	15.3	11.6
CaO	.77	.43– 1.1	.53	.27– .94	5.8	.24	.57	.54
Na_2O	2.65	2.6 – 2.7	1.50	.05– 4.0	12.0	.18	.16	.23
K_2O	2.41	2.2 – 2.7	5.1	3.26– 8.33	11.2	7.8	7.4	6.2
Sum	79.8		84.87			88.8	75.1	89.8

[1]Average of 2 analyses (Y–8–24 and Y–7–148.7).
[2]Average of 8 analyses (2 each from Y–8–24, Y–8–117.1, Y–7–148.8 and Y–7–129).
[3]Homogeneity index (Boyd, 1969), averaged over 8 analyses of green clay. A value larger than 3 indicates inhomogeneous distribution of the constituent.
[4]Total iron as FeO.

mixed-layer montmorillonite-celadonite cannot be established with the microprobe; if they are mixed layers, the scale of mixing is smaller than the resolution of the instrument.

Montmorillonite and occasionally interlayered montmorillonite-celadonite occur in the groundmass, partly replacing clinopyroxene phenocrysts, and in veinlets in the Biscuit Basin flow breccia of Y–7 (table 4), where temperatures are higher than in the sedimentary rocks; celadonite occurs with montmorillonite in this hole at depths below −70 m. Celadonite is commonly the only clay mineral in the Biscuit Basin flow of Y–8, where it occurs along hydration cracks in the altered obsidian and replacing clinopyroxene phenocrysts. Well-crystallized celadonite is the earliest deposited veinlet mineral in the flow breccia of Y–8 (tables 7 and 8).

Celadonite is not abundant in the sedimentary rocks, perhaps because these rocks contain only about 1 percent of total reported iron oxides (table 2), but celadonite is much more abundant in the Biscuit Basin flow, which contains more than 3 percent total iron oxides. The distribution of celadonite in both drill holes is related at least in part to local availability of both ferrous and ferric iron from the rocks. In addition, the greater abundance of celadonite in all units of Y–8 relative to Y–7 suggests that the hotter upflowing waters of Y–8 may be supplying some potassium.

From our few analyses of clay minerals that show wide and apparently unsystematic compositional variations, we do not know whether the clays of one drill hole or the other are consistently higher in K_2O. These clays are poorly crystallized, irregularly interlayered structures that eventually develop into celadonite, but we have no evidence supporting evolution into the illite structure.

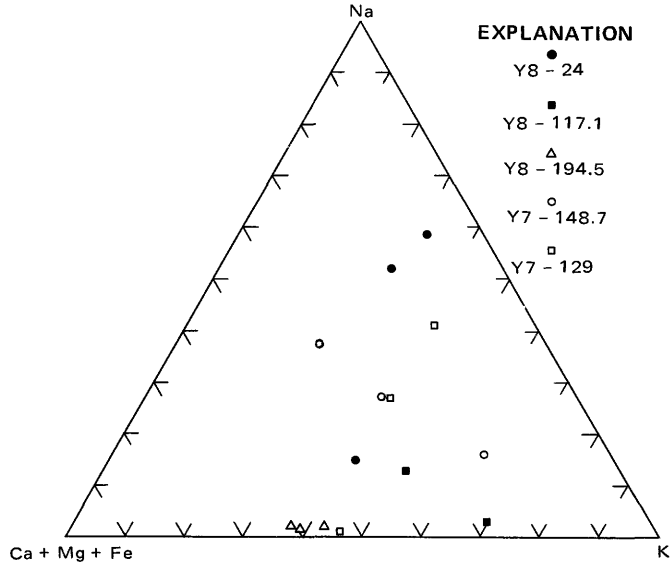

FIGURE 14.—Triangular diagram showing ranges in cation compositions of clay minerals in Y–7 and Y–8.

SILICA MINERALS

The varieties of hydrothermal silica minerals that we recognize include quartz, chalcedony, α-cristobalite (ordered), β-cristobalite (disordered), and opal (X-ray amorphous). Murata and Norman (1976) have recently recognized a complete gradation between well-crystallized quartz and imperfectly crystallized chalcedony and have devised an X-ray method for rating the degree of crystallinity on a scale of 10. Complete gradations are also recognized by Murata and Larson (1975) within the cristobalite series from disordered β-cristobalite to well-ordered α-cristobalite. Murata and Larson (1975) have also noted tridymite as a minor associate of the disordered cristobalite. They recognize no gradation between the amorphous silica of diatomite and the earliest stage of disordered cristobalite, which occurs as a dense rock with few if any relict diatoms. Marked changes in ^{18}O occur during this conversion (Murata and others, 1977), and other marked changes in ^{18}O occur where ordered cristobalite is converted to chalcedony or quartz. These two zones of change indicate extensive reaction between water and solid phases and thus strongly support solution and redeposition. In contrast, no systematic change in ^{18}O occurs during the ordering of cristobalite, or in the stages of conversion of chalcedony to quartz; for these phases, the authors favor solid-state ordering without solution and redeposition.

In the relatively high-temperature, low-pressure, hot-spring environment, a similar series of silica minerals is recognized, but with a few important differences. The freshly deposited sinter, amorphous opal, seems to grade completely into β-cristobalite by means of solid-state ordering with no evidence of solution and redeposition (White and others, 1964; D. E. White, unpub. data). Tridymite has not yet been identified as an associate of β-cristobalite in hydrothermal systems, but instead it occurs only as an early vapor-phase mineral related to initial eruption of lava flows and ash-flow tuffs and not related to the active hydrothermal systems. α-cristobalite is not common in the shallow parts of hot-spring systems, but we have evidence of continuous solid-state ordering between the two recognized cristobalite species in that the major X-ray peak position may range anywhere between 4.11 Å (β-cristobalite) and 4.04 Å (α-cristobalite). Our silica-mineral series agrees with that of Murata and Larson (1975) in requiring solution and redeposition in the

conversion of cristobalite to chalcedony or quartz.

The distribution of the silica minerals in Y–7 and Y–8 is first considered in order of increasing stability. Opal is the dominant silica phase in the hot-spring sinter of both drill holes and is also an abundant cementing mineral of the near-surface sediments; opal is sparse or absent elsewhere throughout the drill holes. At depth, opal occurs only locally in veinlets in the flow breccia of Y–8. Both recognized species of cristobalite are rather erratic in distribution (figs. 3 and 4; tables 5 and 7). β-cristobalite is most common in veinlets in the sediments of Y–7 and in veinlets in the flow breccia of both drill holes. α-cristobalite is present in the groundmass of most core from Y–7 but is absent from significant intervals of Y–8; a few veinlets include α-cristobalite as a relatively early mineral. Chalcedony is very rare in groundmass and veinlets of Y–7 and also in the groundmass of Y–8 but is characteristically the earliest veinlet mineral in the sediments of Y–8. Quartz has not been reported in Y–7 but is sparse to abundant in the groundmass and veinlets of Y–8. Thus, the hotter environment of Y–8 clearly favors quartz and chalcedony, and with rare exceptions these minerals are abundant where opal and β-cristobalite are absent.

This complex picture of the distribution of the silica minerals can best be understood by focusing on their occurrence and relative ages in veinlets. Of the 21 veinlets listed in tables 5 and 7 that have two or more silica species, the relative ages from oldest to youngest in 18 of these are quartz, chalcedony, α-cristobalite, β-cristobalite, and opal; note that this sequence is also in the order of highest to lowest thermodynamic stability. Y–7–209 (−63.7 m) is a probable exception, as are the veinlets from Y–8–185.3 (−56.5 m) and Y–8–197.7 (−60.3 m), where quartz is deposited on chalcedony. The rarity of these exceptions is surprising in view of the common deposition of quartz on chalcedony at a very late stage in cavities in chalcedonic sinter and elsewhere (White and others, 1956).

The usual sequence from most stable to least stable is also in the order of increasing solubility in water at constant temperature (Fournier, 1973). At 100°C, for example, the solubility of quartz is about 50 ppm, chalcedony about 87 ppm, α-cristobalite about 115 ppm, β-cristobalite about 250 ppm, and amorphous silica about 370 ppm. Chemical geothermometers indicate that the thermal waters of Upper Geyser Basin rise to the surface from a reservoir that is probably rather homogeneous at a temperature close to 200°C (Fournier, 1973, p. 134; Fournier and Truesdell, 1973). At 200°C, the solubility of quartz is 260 ppm. With adiabatic cooling (all excess heat converting water to steam) to an eventual surface termperature of 93°C, the maximum content of silica in the residual water is about 330 ppm; if boiled to an intermediate stage of adiabatic cooling at 150°C, the residual water has 290 ppm of silica. From these relations, we conclude that water from the reservoir is strongly supersaturated with respect to quartz, chalcedony, and α-cristobalite at all temperatures in the drill holes, but is only slightly supersaturated with respect to β-cristobalite and is unsaturated with respect to opal at all temperatures higher than about 80°C (at depths below −15 m in Y–7 and −6 m in Y–8).

The indicated occurrence of opal at temperatures as high as 140°C in Y–7 and 170°C in Y–8 is inconsistent with these conclusions. Three possible explanations are: (1) the deep opal was deposited when reservoir temperatures and the silica contents of upflowing water were much higher; conversion to cristobalite has not yet occurred; (2) the deep opal is everywhere associated with undevitrified obsidian, which could have a solubility as high as that of amorphous silica (R.O. Fournier, oral commun., 1976); the hot water has locally equilibrated with obsidian and has then risen and cooled enough to deposit opal; or (3) the deep opal identified only by its optical properties (isotropic; index of refraction about 1.46), is nowhere abundant enough to isolate and confirm as being amorphous by X-ray; it may actually be isotropic β-cristobalite of low crystallinity. We suspect, but cannot prove, that the third alternative is correct.

How are the two strong tendencies for paragenesis from most stable to least stable, and for mutual exclusion of quartz and chalcedony from cristobalite and opal, best reconciled? Were all silica minerals initially deposited in their present form or does the sequence indicate conversion through time from less stable forms to more stable forms? White, Brannock and Murata (1956) and Murata and Larson (1975) have concluded that each silica mineral forms from water only slightly supersaturated with respect to that mineral; a water supersaturated with respect to opal tends to precipitate opal and not other forms, and a chalcedony-supersaturated water does not precipitate quartz. If this concept is valid, the present mineral assemblages are best explained by consistently high silica contents in the waters of the main upflow channels, but with eventual self-sealing and isolation of individual small channels, veinlets, and rock masses. With such isolation, or semi-isolation, each unit of rock volume can then behave much like a closed system, with pore water evolving toward lower silica contents as more stable silica minerals are in succession reconstituted from less stable minerals. With respect to each successive mineral, the pore water is successively supersaturated, just saturated, and then undersatu-

rated, starting with the least stable silica mineral that can precipitate and evolving toward the more stable, with each requiring a lower silica content in the water. This model of evolution implies, for example, that the sequence from −41 to −55 m in Y–8 (generally with quartz as the only silica mineral) has either been an isolated closed system throughout recent activity or, as a favored alternate possibility, this interval was only semiclosed, permitting limited inflow of high-silica water that mixed convectively with lower-silica water already adjusted to the mineral assemblage of the unit. The limited inflow of new silica permits continuing precipitation of quartz, but saturation with respect to chalcedony is not ordinarily reached (in the profile of the drill hole).

ZEOLITES

In order to understand interrelations of the zeolites, their chemical composition is critical but also difficult to obtain. Electron microprobe analysis, which is the best available method for fine-grained intermixtures, is often unsatisfactory and frustrating to the analyst. A low beam current and a slightly defocused beam (about 10μm) are usually used to keep the sample from volatilizing. In addition, each grain has a large $\frac{\sigma}{\sqrt{N}}$ (table 9), indicating that all elements other than calcium are inhomogeneously distributed. Also, most grains are so small that only a few separate spots can be counted in each grain, making a statement of precision meaningless.

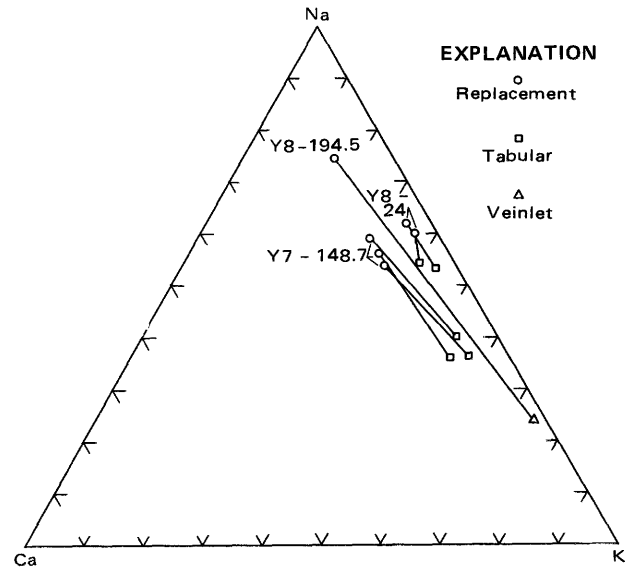

FIGURE 15.—Triangular diagram showing cation compositions of clinoptilolite in Y–7 and Y–8. Tie lines represent analyses of clinoptilolite replacing glass and of recrystallized (tabular) clinoptilolite from the same sample; sample numbers indicate depth (in feet).

Individual electron microprobe analyses are averaged in table 9 and are plotted in figure 15. The calcium content of clinoptilolite from Y–7 is greater than that from Y–8 in both replacement and tabular types. The clinoptilolite deposited as tabular euhedral crys-

TABLE 9.—*Electron microprobe analyses of zeolites from Y–7 and Y–8*
[Analyst: M. H. Beeson. Looked for but not found: Ba]

	Y–8–117.1 Analcime	Y–7–148.7[1] Replacement clinoptilolite	Y–7–148.7[1] Tabular clinoptilolite	Y–8–24[1] Replacement clinoptilolite	Y–8–24[1] Tabular clinoptilolite	Y–8–194.5 Veinlet clinoptilolite	Av $\frac{\sigma}{\sqrt{N}}$ *
SiO_2	59.79	71.9	67.1	66.3	70.3	75.3	4.6
Al_2O_3	18.36	10.3	11.4	12.1	11.9	8.9	3.4
CaO	.00	1.21	.82	.54	.45	.13	2.1
Na_2O	10.83	3.22	2.03	4.42	2.64	1.23	11.6
K_2O	.00	3.09	4.28	3.87	3.11	5.73	8.7
Sum	88.98	89.7	85.6	87.0	88.4	91.3	
Ions/formula based on 72 oxygens							
Si	26.49	30.81	30.20	29.58	30.38	31.64	
Al	9.59	5.20	6.07	6.38	6.05	4.42	
Ca	.00	.56	.40	.26	.21	.06	
Na	9.31	2.67	1.76	3.95	2.22	1.00	
K	.00	1.42	2.45	2.20	1.73	3.07	
$\frac{2Ca+Na+K}{Al}$	1.029	1.004	.824	1.026	.811	.9357	
Si/Al	2.76	5.93	4.98	4.64	5.02	7.16	
An	------	12.0	8.6	4.2	5.1	1.4	
Ab	100.0	57.6	38.2	61.0	53.5	24.3	
Or	------	30.6	53.2	34.8	41.4	74.3	

[1]Average of 2 analyses.
*Homogeneity index (Boyd, 1969) averaged over all analyses of each sample. A value larger than 3 indicates that a particular element has an inhomogeneous distribution.

tals in open spaces and pores is enriched in K_2O over that replacing obsidian, especially that from Y–7. The one analyzed clinoptilolite from a veinlet in Y–8 is even higher in K_2O with 5.73 percent. To our knowledge, clinoptilolite with such high K_2O content has not been reported previously, but Sheppard, Gude, and Munson (1965) found diagenetic clinoptilolites that ranged from 3.86 to 5.43 percent K_2O in tuffacous rocks of the Mojave Desert, and Kashkai and Babaev (1976) report a clinoptilolite containing 5.30 percent K_2O from a zeolitized tuff from the Aydag deposit in the Azerbaidzhan SSR.

Analcime is absent from Y–7 but is abundant in parts of Y–8, where it occurs in contact with clinoptilolite on the borders of alternating thin bands in the upper 24.4 m (fig. 4). Elsewhere in Y–8 the two are mutually exclusive, with analcime everywhere occurring with quartz, and clinoptilolite nearly everywhere being associated with one or more of the less stable forms of silica, usually α-cristobalite. The strong tendencies for analcime to be associated with quartz and for these two minerals to occur without clinoptilolite and the less stable silica minerals were emphasized by Honda and Muffler (1970) as being characteristic of Y–1, with most exceptions also occurring in the upper part of that drill hole.

Considering analyses of all zeolite species, clinoptilolite, although variable, tends to be relatively high in silica, and analcime, which is also variable, is lower in silica. All of the clinoptilolites of Y–7 and Y–8 are the high-silica varieties. A representative analcime sample from Y–8 is a pure sodium variety with a silica-to-alumina ratio of 2.76:1, which is very high for analcime (table 9; the ratio in common analcime is close to 2:1). The high silica content is consistent with the relations between the silica minerals and silica contents of the pore water, as previously discussed, in that the lower silica phase (analcime) is not deposited if the fluid is supersaturated with respect to the higher silica phase (clinoptilolite).

Mordenite coexists with clinoptilolite and to a lesser extent with analcime and is also intermediate between the two in relative silica content. If silica content were the only controlling factor, we might also expect mordenite to be intermediate in time of deposition. Where age relations can be deciphered with confidence (tables 5 and 7), mordenite does follow clinoptilolite but, for reasons that are not evident, mordenite also occurs after analcime as a partial filling of open spaces in veinlets and pores. Several attempts were made to analyze mordenite with the electron microprobe, but even with a very low sample current and a defocused beam, the mineral volatilized too rapidly for satisfactory analysis.

POTASSIUM FELDSPAR

Hydrothermal potassium feldspar, as in other hot-spring systems, is monoclinic; from its optical and electron microprobe compositions, it is chemically near the pure potassium end member. Potassium feldspar is a minor but persistent mineral in the alteration of Y–8, where it is associated with quartz and analcime zones in the altered sediments at depths below −24.8 m, and is also present in minor amounts throughout the Biscuit Basin flow. It has not been found in core from Y–7 or in veinlets from Y–8. For comparison, a little hydrothermal potassium feldspar was found in Y–1 (Honda and Muffler, 1970), and it is relatively abundant in veinlets and groundmass from Carnegie–I drill hole of the Myriad group of Upper Geyser Basin (Fenner, 1936; confirmed in Fenner's core by present authors).

Hydrothermal potassium feldspar is given special prominence by Browne and Ellis (1970) in their study of core and cuttings from the Broadlands system of New Zealand. They conclude that hydrothermal potassium feldspar indicates the permeable upflow channels of the hottest water, which is usually highest in potassium. With decreasing pressure the water boils, losing CO_2 to the vapor phase, thereby increasing the pH and the K/H ratio and shifting the water into the potassium feldspar stability field (Hemley and Jones, 1964). In general we agree with these conclusions, which provide an excellent explanation for the relatively abundant potassium feldspar in Carnegie–I drill hole and in Yellowstone's Y–13 drill hole (T. E. C. Keith, unpub. data; White and others, 1975, p. 41–45). However, the uniform distribution of minor potassium feldspar in Y–8 (fig. 4) is better explained as a product of the conversion of clinoptilolite to analcime. Clinoptilolite is one of the few zeolites that readily accepts potassium and may contain as much as 5.73 percent K_2O (table 9). In contrast, analcime is consistently low in potassium (except for phenocryst analcime in high-potassium volcanic rocks). This contrast suggests that as clinoptilolite high in potassium is converted to analcime, the excess potassium precipitates in part as potassium feldspar. The close relation of potassium feldspar to analcime (fig. 4) and to the absence of clinoptilolite is thereby explained. Much of the potassium in the original rocks is also fixed in the clay minerals, to some extent as montmorillonite and mixed-layer clays but to a greater extent as celadonite (table 8). However, none of these potassium-bearing clays seems to increase in abundance as potassium is released in reconstituting clinoptilolite to analcime.

The whole-rock chemical compositions of the two zeolitic assemblages differ considerably, with enrichment of Na_2O and decrease of K_2O in the analcime-rich

sediments relative to the clinoptilolite-rich sediments (table 3). However, the analcime-rich sediments below −35.7 m, in which potassium feldspar crystals are common, have a considerably higher proportion of K_2O than in analcime-rich rocks without hydrothermal potassium feldspar (compare analyses Y–8–32.5 (−9.9 m) and Y–8–160.5 (−48.9 m) of table 2). Table 3 also shows higher Al_2O_3 and slightly lower SiO_2 and CaO in the analcime-rich sediments with no hydrothermal potassium feldspar.

CALCITE

Calcite is absent or very rare in Y–7 but is common in parts of the sedimentary section of Y–8. Two habits are recognized in Y–8; rhombic calcite is the latest mineral in some veinlets from −9.8 to −21.3 m, and bladed calcite, also as the latest mineral, occurs in veinlets and groundmass from about −50 to −55 m in the lower part of the quartz-analcime-potassium feldspar zone previously discussed.

If other parameters are constant, the solubility of calcite increases with decreasing temperature. In general, we view the scarcity of calcite as due to decreasing temperature upward in the principal flow channels. Precipitation of calcite can be due to several different circumstances; an especially important one in Yellowstone National Park is related to the high fluid overpressures at depth, with boiling occurring as pressures decrease irregularly upward (White and others, 1975). The depth of the most rapid pressure change in Y–8 cannot be determined precisely from the physical data but is close to −55 m, where fluid overpressures decreased abruptly upward from about +2.2 kg/cm² to +0.6 kg/cm² (White and others, 1975, p. 18–19). Water flowing upward through a restricted channel at a temperature near 168°C and a pressure near 2.2 kg/cm² is about 11°C above boiling when its pressure suddenly decreases to 0.6 kg/cm² (White and others, 1975, p. 18–19). About 2 percent of the water is suddenly boiled to steam, and CO_2 is selectively lost to the vapor phase, consequently increasing the pH, converting bicarbonate to carbonate, and precipitating calcite.

RELATIVE IMPORTANCE OF TEMPERATURE AND FLUID COMPOSITIONS

We conclude, in agreement with Honda and Muffler (1970), that the mineral associations of Y–7 and Y–8 cannot be explained by temperature differences alone, even though temperature is obviously important. We have already cited the outstanding demands for more than temperature alone: (1) the distribution of undevitrified obsidian, still prevalent at or near the maximum temperatures of each hole; (2) coexistence or close association of minerals that are obviously not in equilibrium with each other, including various combinations of silica minerals; (3) temperature-independent alternation of clinoptilolite-cristobalite and analcime-quartz with depth.

Erionite occurs in only one sample from about −4.9 m in Y–8 (fig. 4), where its temperature of formation was probably between 75 and 80°C. Erionite with similar limited distribution was also suspected by Honda and Muffler (1970) to be restricted to low temperatures; the maximum temperature of formation at which erionite was observed in Y–1 was about 110°C.

Laumontite is a relatively rare zeolite in siliceous low-calcium geothermal systems. Its scarcity in the Upper Geyser Basin drill holes may be more closely related to the low availability of calcium than to temperature restrictions; all laumontite of Y–8 occurs in veinlets at temperatures near 170°C.

Honda and Muffler (1970) found that obsidian as well as opal and β-cristobalite occurred in Y–1 at temperatures of less than about 110°C, but these restrictions are not effective in Y–7 and Y–8, where environments of these minerals are as hot as 170°C. Y–1 was clearly much more permeable than Y–7 and Y–8, and hence opal and β-cristobalite would be less likely to persist. Chlorite may be favored by high temperature, but relative scarcity of magnesium and ferrous iron in the altering rocks is likely to be more important. Celadonite is absent from the sedimentary rocks of Y–7, where temperatures range up to 117°C, but occurs at higher temperatures in the underlying Biscuit Basin flow. In Y–8, celadonite occurs in all rocks deeper that −7.6 m and at temperatures above 80°C and is especially abundant in the Biscuit Basin flow. These data indicate that availability of magnesium and iron is clearly important, judging from the abundance of celadonite in the Biscuit Basin flow of both drill holes as compared to the overlying sediments, which are lower in these elements (table 2).

Thus, many chemical reactions occurring in these rocks are favored by high temperature, but permeability and an adequate supply of through-flowing fluids seem to be equally important for most reactions in supplying some constituents and redistributing or removing others. Our conclusions are nearly identical to those of Honda and Muffler (1970).

SUMMARY OF EVIDENCE FOR SELF-SEALING

The physical evidence for self-sealing of the original sediments of Y–7 and Y–8 was reviewed by White and others (1975, p. 22). In summary, the original sediments (as interpreted from drill core) contain no strata likely to have been initially so fine grained and low enough in permeability to account for the observed ver-

tical pressure differences (core recovery through the sedimentary section was 76 percent from Y–7 and 88 percent from Y–8). However, the lithologies as represented by patterns in figures 3 and 4 have correlative zones near −15 m and from −21.3 to −27.4 m that contain silt-sized clastic sediments of moderately low initial permeability, thus decreasing bulk vertical permeability.

Strong evidence for horizontal self-sealing by hydrothermal alteration and mineral deposition exists in the contrasts in wellhead water pressure between Y–8 and Y–7 at equivalent depths. All of the sediments were rather well sorted by streams, and the coarser clastic zones are correlative between the two holes (fig. 3 and 4). The depth ranges of individual zones in the two holes are (in meters, with Y–8 listed first): (1) 1.5–8.5 and 4.0–7.0; (2) 25.3–28.4 and 23.5–24.4; (3) 35.1–36.3 and 32.0–32.6; (4) 41.2–42.7 and 40.2–42.7; (5) 47.6–54.9 and 44.8–48.2 (and probably to 52.7 but no core was recovered). If the depth intervals are corrected for differences in wellhead altitude, with Y–7 being 1.8 m lower than Y–8, the gravel zones are at almost the same altitude. If these zones are assumed to be both correlative and originally permeable, the large pressure differences observed today between the two holes provide convincing physical evidence for self-sealing. The pressure difference in the basal sediments from Y–8 to Y–7 is now about 1.49 kg/cm^2 per 100 m, or a gradient of 0.17, with pressure converted to equivalent meters of water (White and others, 1975, p. 22). In contrast, the pressure gradient from Y–7 to the Firehole River, both of which are outside of the principal area of self-sealing, is only about 0.01.

The photographic evidence in this report demonstrates extensive dissolution of obsidian granules. Some of the reconstituted new minerals were deposited in the relict granule spaces, but probably an equal fraction was deposited in the pore spaces between granules. For any specific sample, we cannot determine with certainty whether an interstitial space was originally a void or whether the sediments were initially poorly sorted with fine clastic grains interstitial to the larger grains, and now completely destroyed. The present sediments of unaltered kame terraces of the Upper Geyser Basin (Waldrop, 1975) are considered to be equivalent to the original sediments of the drill holes. These obsidian-bearing sands and gravels are so porous and open textured that, except locally, precipitation does not drain off in surface channels and gullies but sinks underground. Thus, the total physical, chemical, and petrographic evidence points conclusively to hydrothermal self-sealing as an important near-surface factor in the development and evolution of this geothermal system.

REFERENCES CITED

Bodvarsson, Gunnar, 1964, Physical characteristics of natural heat resources in Iceland, *in* Geothermal energy I: United Nations Conf. New Sources Energy, Rome, 1961, Proc., v. 2, p. 82–90.

Boyd, F. R., 1969, Electron-probe study of diopside inclusions from kimberlite: Am. Jour. Sci., v. 267–A, p. 50–64.

Browne, P. R. L., and Ellis, A. J., 1970, The Ohaki-Broadlands hydrothermal area, New Zealand: Mineralogy and related geochemistry: Am. Jour. Sci., v. 269, p. 97–131.

Christiansen, R. L., and Blank, H. R., Jr., 1972, Volcanic stratigraphy of the Quaternary rhyolite plateau in Yellowstone National Park: U.S. Geol. Survey Prof. Paper 729–B, 18 p.

———1974, Geologic map of the Old Faithful quadrangle, Yellowstone National Park, Wyoming: U.S. Geol. Survey Map GQ–1189, scale 1:62,500.

Dunbar, C.O., and Rodgers, John, 1951, Principles of stratigraphy: New York, John Wiley and Sons, 356 p.

Facca, Giancarlo, and Tonani, Franco, 1967, The self-sealing geothermal field: Bull. Volcanol., v. 30, p. 271–273.

Fenner, C. N., 1936, Bore-hole investigations in Yellowstone National Park: Jour. Geology, v. 44, p. 225–315.

Fournier, R. O., 1973, Silica in thermal waters: Laboratory and field investigations, *in* International Symposium on Hydrogeochemistry and Biogeochemistry Proceedings, Tokyo, 1970, v. 1, Hydrogeochemistry: Washington, D. C., Clark, p. 122–139.

Fournier, R. O., and Truesdell, A. H., 1973, An empirical Na-K-Ca geothermometer for natural waters: Geochim. et Cosmochim. Acta, v. 37, p. 1255–1275.

Friedman, Irving, and Smith, R. L., 1958, The deuterium content of water in some volcanic glasses: Geochim. et Cosmochim. Acta, v. 15, p. 218–228.

Hemley, J. J., and Jones, W. R., 1964, Aspects of the chemistry of hydrothermal alteration with emphasis on hydrogen metasomatism: Econ. Geology, v. 59, p. 538–569.

Honda, S., and Muffler, L. J. P., 1970, Hydrothermal alteration in core from research drill hole Y–1, Upper Geyser Basin, Yellowstone National Park, Wyoming: Am. Mineralogist, v. 55, p. 1714–1737.

Kashkai, M.-A., and Babaev, I. A., 1976, Clinoptilolite from zeolitized tuffs of Azerbaidzhan: Mineral. Mag., v. 40, p. 501–511.

Murata, K. J., and Larson, R. R., 1975, Diagenesis of Miocene siliceous shales, Temblor Range, California: U.S. Geol. Survey Jour. Research, v. 3, p. 553–566.

Murata, K. J., Friedman, Irving, and Gleason, J. D., 1977, Oxygen isotope relations between diagenetic silica minerals in Monterey Shale, Temblor Range, California: Am. Jour. Sci., v. 277, p. 259–272.

Murata, K. J., and Norman, M. B., II, 1976, An index of crystallinity for quartz: Am. Jour. Sci., v. 276, p. 1120–1130.

Pierce, K. L., Obradovich, J. D., and Friedman, Irving, 1976, Obsidian hydration dating and correlation of Bull Lake and Pinedale Glaciations near West Yellowstone, Montana: Geol. Soc. America Bull., v. 87, p. 703–710.

Shapiro, Leonard, 1967, Rapid analysis of rocks and minerals by a single-solution method: U.S. Geol. Survey Prof. Paper 575–B, p. B187–B191.

Sheppard, R. A., Gude, A. J., III, and Munson, E. L., 1965, Chemical composition of diagenetic zeolites from tuffaceous rocks of the Mojave Desert and vicinity, California: Am. Mineralogist, v. 50, p. 244–249.

Smith, J. R., and Yoder, H. S., Jr., 1956, Variations in X-ray powder diffraction patterns of plagioclase feldspars: Am. Mineralogist, v. 41, p. 632–647.

Waldrop, H. A., 1975, Surficial geologic map of the Old Faithful quadrangle, Yellowstone National Park, Wyoming: U.S. Geol. Survey Map I–649, scale 1:62,500.

White, D. E., Brannock, W. W., and Murata, K. J., 1956, Silica in hot-spring waters: Geochim. et Cosmochim. Acta, v. 10, p. 27–59.

White, D. E., Fournier, R. O., Muffler, L. J. P., and Truesdell, A. H., 1975, Physical results of research drilling in thermal areas of Yellowstone National Park, Wyoming: U.S. Geol. Survey Prof. Paper 892, 70 p.

White, D. E., Thompson, G. A., and Sandberg, C. H., 1964, Rocks, structure, and geologic history of Steamboat Springs thermal area, Washoe County, Nevada: U.S. Geol. Survey Prof. Paper 458–B, 63 p.

Yakowitz, H., Myklebust, R. L., and Heinrich, K. F. J., 1973, FRAME: An on-line correction procedure for quantitative electron probe microanalysis: U.S. Natl. Bur. Standards Tech. Note 796, 47 p.

☆ U.S. GOVERNMENT PRINTING OFFICE: 1978 - 789-107/63 9-II